VTRC Virginia Transportation Research Council

We Bring Innovation to Transportation

Carbon Fiber Reinforced Polymer (CFRP) for Pretension Applications: Material Acceptance Criteria and Advancing Anchorage Designs

http://www.virginiadot.org/vtrc/main/online_reports/pdf/20-r5.pdf

JONATHON D. TANKS, E.I.T.
Graduate Research Assistant
Virginia Transportation Research Council

STEPHEN R. SHARP, Ph.D., P.E.
Senior Research Scientist
Virginia Transportation Research Council

H. CELIK OZYILDIRIM, Ph.D., P.E.
Principal Research Scientist
Virginia Transportation Research Council

DEVIN K. HARRIS, Ph.D.
Assistant Professor
Department of Civil and Environmental Engineering
University of Virginia

Final Report VTRC 20-R5

VIRGINIA TRANSPORTATION RESEARCH COUNCIL
530 Edgemont Road, Charlottesville, VA 22903-2454
vtrc.virginiadot.org

Standard Title Page—Report on State Project

Report No.: VTRC 20-R5	Report Date: October 2019	No. Pages: 50	Type Report: Final	Project No.: RC 00068
			Period Covered:	Contract No.:

Title:
Carbon Fiber Reinforced Polymer (CFRP) for Pretension Applications: Material Acceptance Criteria and Advancing Anchorage Designs

Key Words: CFRP, QA/QC CFRP, anchorage, wedge, concrete, prestressed, carbon fiber, corrosion, reinforcement

Author(s):
Jonathon D. Tanks, E.I.T., Stephen R. Sharp, Ph.D., P.E., H. Celik Ozyildirim, Ph.D., P.E., and Devin K. Harris, Ph.D.

Performing Organization Name and Address:
Virginia Transportation Research Council
530 Edgemont Road
Charlottesville, VA 22903

Sponsoring Agencies' Name and Address:
Virginia Department of Transportation
1401 E. Broad Street
Richmond, VA 23219

Supplementary Notes:

Abstract:

One of the main causes of structural deficiency in concrete bridges is the deterioration of the constituent materials. In order to achieve the goal of a design life of 75 to 100 years, it is imperative that pretensioned elements—girders, piles, and deck panels—contain corrosion-resistant or corrosion-free strands. The Virginia Department of Transportation (VDOT) is using carbon fiber reinforced polymers (CFRP) as a corrosion-free alternative to steel prestressing materials for longer lasting concrete bridge structures in Virginia. The in-service performance of elements can be difficult to evaluate in certain structural applications, such as pretensioned concrete bridges, where instrumentation is often limited and the material cannot be removed for inspection; use of corrosion-free CFRP will eliminate corrosion, the most common deterioration mechanism in reinforced elements.

To implement CFRP in pretensioned concrete bridge structures with more confidence, this study was initiated to examine issues pertaining to material durability and quality control, laboratory testing procedures, and improved pretensioning anchorage systems. The experimental approach was intended to establish a testing methodology that can be adopted by VDOT for evaluating the quality and durability of CFRP in concrete structures.

Several conclusions were drawn from the results of this study: (1) mechanical testing is important for characterizing CFRP prestressing material and should be supported by analysis of physical and thermal properties; (2) short-term preloading of the CFRP to 75% of the ultimate tensile strength has a significant impact on durability compared to unstressed material and higher temperatures accelerate degradation; and (3) a promising anchorage prototype was designed for improving pretensioning operations when using CFRP.

The study recommends that VDOT's Materials Division prepare guidelines for checking the durability of CFRP reinforcement. Further, the manufacturers of the composite materials should provide data indicating conformance with the guidelines. In addition, the Virginia Transportation Research Council should continue work on the development of an improved wedge system for CFRP. This wedge would increase production rates during pretensioning and allow for easier use in post-tensioning applications. It is also possible that this wedge could be used for stainless steel strand.

FINAL REPORT

CARBON FIBER REINFORCED POLYMER (CFRP) FOR PRETENSION APPLICATIONS: MATERIAL ACCEPTANCE CRITERIA AND ADVANCING ANCHORAGE DESIGNS

Jonathon D. Tanks, E.I.T.
Graduate Research Assistant
Virginia Transportation Research Council

Stephen R. Sharp, Ph.D., P.E.
Senior Research Scientist
Virginia Transportation Research Council

H. Celik Ozyildirim, Ph.D., P.E.
Principal Research Scientist
Virginia Transportation Research Council

Devin K. Harris, Ph.D.
Assistant Professor
Department of Civil and Environmental Engineering
University of Virginia

Virginia Transportation Research Council
(A partnership of the Virginia Department of Transportation
and the University of Virginia since 1948)

Charlottesville, Virginia

October 2019
VTRC 20-R5

DISCLAIMER

The contents of this report reflect the views of the authors, who are responsible for the facts and the accuracy of the data presented herein. The contents do not necessarily reflect the official views or policies of the Virginia Department of Transportation, the Commonwealth Transportation Board, or the Federal Highway Administration. This report does not constitute a standard, specification, or regulation. Any inclusion of manufacturer names, trade names, or trademarks is for identification purposes only and is not to be considered an endorsement.

ABSTRACT

One of the main causes of structural deficiency in concrete bridges is the deterioration of the constituent materials. In order to achieve the goal of a design life of 75 to 100 years, it is imperative that pretensioned elements—girders, piles, and deck panels—contain corrosion-resistant or corrosion-free strands. The Virginia Department of Transportation (VDOT) is using carbon fiber reinforced polymers (CFRP) as a corrosion-free alternative to steel prestressing materials for longer lasting concrete bridge structures in Virginia. The in-service performance of elements can be difficult to evaluate in certain structural applications, such as pretensioned concrete bridges, where instrumentation is often limited and the material cannot be removed for inspection; use of corrosion-free CFRP will eliminate corrosion, the most common deterioration mechanism in reinforced elements.

To implement CFRP in pretensioned concrete bridge structures with more confidence, this study was initiated to examine issues pertaining to material durability and quality control, laboratory testing procedures, and improved pretensioning anchorage systems. The experimental approach was intended to establish a testing methodology that can be adopted by VDOT for evaluating the quality and durability of CFRP in concrete structures.

Several conclusions were drawn from the results of this study: (1) mechanical testing is important for characterizing CFRP prestressing material and should be supported by analysis of physical and thermal properties; (2) short-term preloading of the CFRP to 75% of the ultimate tensile strength has a significant impact on durability compared to unstressed material and higher temperatures accelerate degradation; and (3) a promising anchorage prototype was designed for improving pretensioning operations when using CFRP.

The study recommends that VDOT's Materials Division prepare guidelines for checking the durability of CFRP reinforcement. Further, the manufacturers of the composite materials should provide data indicating conformance with the guidelines. In addition, the Virginia Transportation Research Council should continue work on the development of an improved wedge system for CFRP. This wedge would increase production rates during pretensioning and allow for easier use in post-tensioning applications. It is also possible that this wedge could be used for stainless steel strand.

FINAL REPORT

CARBON FIBER REINFORCED POLYMER (CFRP) FOR PRETENSION APPLICATIONS: MATERIAL ACCEPTANCE CRITERIA AND ADVANCING ANCHORAGE DESIGNS

Jonathon D. Tanks, E.I.T.
Graduate Research Assistant
Virginia Transportation Research Council

Stephen R. Sharp, Ph.D., P.E.
Senior Research Scientist
Virginia Transportation Research Council

H. Celik Ozyildirim, Ph.D., P.E.
Principal Research Scientist
Virginia Transportation Research Council

Devin K. Harris, Ph.D.
Assistant Professor
Department of Civil and Environmental Engineering
University of Virginia

INTRODUCTION

Although concrete can undergo deterioration mechanisms such as service load cracking, scaling, and delamination, one of the leading causes of reinforced concrete deterioration is corrosion of steel reinforcement (Hartt and Rapa, 1998). Corrosion can also degrade steel subjected to high levels of sustained stress, such as seven-wire prestressed concrete steel strand, that provides a critical function in structural elements. This can lead to unexpected maintenance costs, with the difference in the life cycle cost of using a more corrosion-resistant material greatly reduced after the first maintenance operation (Grace et al., 2012; Sharp and Moruza, 2009).

An example of corrosive attack on post-tensioning steel strands is shown in Figure 1. In this figure, corrosion resulted in the failure of a single 19-strand tendon and the loss of steel cross-section on other tendon wires. This continues to be an issue, as poor quality grout can lead to corrosion of the steel. Some departments of transportation (DOTs) have switched from grout to unbonded wax filler to protect the steel from corrosion (Cox, 2017; Sprinkel, 2015; Sprinkel and Balakumaran, 2017). Pretensioning elements have also exhibited corrosion damage in the field. Figure 2 shows the loss of pretensioning strands along the bottom of a set of beams attributable to a leaking joint.

(a) (b)

Figure 1. Corrosive Attack on Post-Tensioned Structural Strand: (a) corrosion of individual strand wires ultimately causing an overload failure of the middle external tendon (orange arrow); middle tendon is hanging by the broken wires inside the other half of the duct; (b) section loss in high-strength steel strand, with red arrows showing ends of a fractured wire

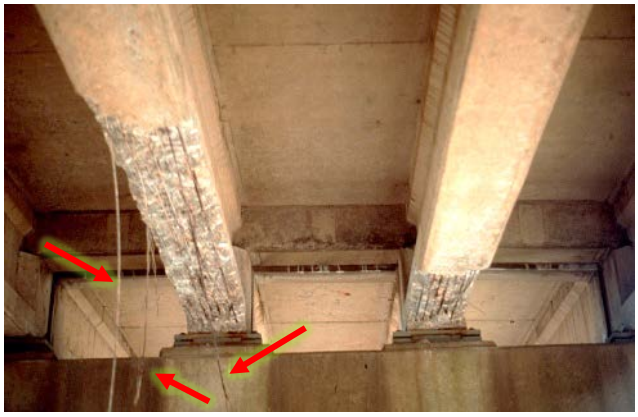

Figure 2. Failure of Corroded Conventional Steel Strands. Some have snapped and now hang down (red arrows) along the bottom of several beams because of leaking bridge deck joints.

Recognizing the need to reduce maintenance costs and extend the service life of bridges, the Virginia Department of Transportation (VDOT) incorporated corrosion-resistant materials in its structures. For example, VDOT has transitioned from epoxy-coated reinforcement to corrosion-resistant reinforcement in decks. However, in order to achieve the goal of a design life of 75 to 100 years, it is imperative that pretensioned and post-tensioned elements—girders, piles, and deck panels—also contain either corrosion-resistant or corrosion-free strands.

Fiber Reinforced Polymer Materials

Fiber reinforced polymer (FRP) composites have become more popular as a corrosion-free, lightweight alternative to steel. These materials are multiphase systems that are designed to bear physical loads in structures; they consist of a reinforcing phase (fibers) and a matrix phase (polymer) that are bound together through chemical adhesion (interface). Despite the many advantages of composites, FRP composites can be susceptible to degradation when subjected to

certain environmental and loading conditions. This is because the polymer matrix tends to be a material that is sensitive to moisture, heat, stress, and chemicals.

Upon mechanical loading of a material, pathways that facilitate the movement of solutions through the FRP composite are made possible because of matrix microcracking. Assuming that the interfacial bond strength is not deficient, matrix microcracking is the first type of damage to occur in FRP from mechanical loading. These pathways allow moisture to transport via capillary flow more easily than bulk diffusion. This results in a greater degree of penetration of the aqueous solutions. This is important to consider in the case of FRP composites that carry high levels of stress. As Tanks et al. (2017a) indicated, this FRP response to loading can alter the properties of FRP material and decrease the durability.

DOTs and Carbon Fiber Reinforced Polymer

Several DOTs, listed in Table 1, have used carbon fiber reinforced polymer (CFRP) strands in pretensioned bridge elements, mainly prestressed concrete beams and piles, in an effort to reduce corrosion damage. This list has continued to grow, with several more in progress in the United States.

Starting in 2012 and continuing to date, VDOT has been pursuing CFRP as a corrosion-free alternative to steel prestressing materials for longer lasting concrete bridge structures in Virginia. In the Nimmo Parkway Bridge (Virginia Beach), there are 18 concrete piles pretensioned with a seven-wire CFRP strand product named carbon fiber composite cable (CFCC) by the manufacturer (Ozyildirim and Sharp, 2014). Now, with more use of FRP materials by DOTs, a sound and repeatable testing protocol is needed for evaluating CFRP durability in the laboratory as part of the criteria for use in concrete bridge structures (American Concrete Institute [ACI], 2014). In addition, the end preparation for anchorage is time-consuming and delays the fabrication process, missing the daily production cycles. Improvements to current protocols could help researchers, designers, and DOTs incorporate CFRP in bridges more easily and with greater confidence.

PURPOSE AND SCOPE

This study was initiated after several shortcomings that currently limit the widespread use of CFRP in prestress applications were detected. DOTs do not have a uniform baseline set of strand qualification and verification test procedures to facilitate acceptance, and observations in the field indicated that the preparation time required for prestress anchorage systems is slow. Improvements in both of these areas could help reduce the cost of using this technology and promote competition. The primary objectives of this study, therefore, were as follows:

1. Establish a clear set of tests for CFRP quality acceptance (QA) and quality control (QC) for prestressing applications that can be adopted by VDOT and other states by either modifying existing standards or creating new guidelines

2. Survey current pretensioning anchorage systems for CFRP, and evaluate the feasibility of developing a new prototype that has the potential to reduce labor and preparation time at precast plants.

Table 1. Selected Projects Using CFRP Strand in North American Bridges

DOT	Structure	Application	Element	Diameter, in (mm)	Element Dimension, ft	Year
Colorado [a]	I-225/Parker Road Bridge	Pre-tensioning	Precast Panels	0.39 (10) CFRP 0.5 (13) GFRP	9 2/3	2001
Kentucky [b]	KY70 Bridge	Pre-tensioning	Beam	0.6 (15.2)	~77	2014
Maine [c]	Penobscot Narrows Bridge	Post-tensioning	Stay Cable	0.60 (15.2) strand 37 strands per cable	Stay 2: 134 and 149; Stay 10: 303 and 346; Stay 17: 459 and 526	2007
Manitoba [d]	Taylor Bridge	Pre-tensioning	Beams	Unk.	~108	1998
Michigan [e]	Bridge St. Bridge	Pre- and post-tensioning	Beam	0.4 (10) Internal Tendon 1.6 (40) External Strand	69	2001
Michigan [f]	Pembroke Bridge	Post-tensioning	Beams	1.6 (40)	Unk.	2011
Michigan [b]	M102 Bridges	Pre-tensioning	Beam	0.6 (15.2)	~62	2013-2014
Michigan [b]	I-94 Bridges	Post-tensioning	Beam	1.6 (40)	~58 and ~62	2014-2015
Missouri [a]	Southview Dr. Bridge	Pre-tensioning	Deck	3/8	40	2005
Ohio [b]	Route 79 Bridge	Post-tensioning	Beam	Unk.	Unk.	Unk.
Virginia [f]	Nimmo Parkway Bridge	Pre-tensioning	Piles	0.6 (15.2) 0.2 (5.7)	24-in-square pile, 76 ft long	2014
Virginia [f]	Route 49 Bridge	Pre-tensioning	Beams	0.6 (15.2) 0.68 (17.2)	45 in tall 84 ft long	2015
Virginia [g]	Laskin Road Bridge (Proposed)	Pre-tensioning	Piles	Not fabricated at time of publication	Not fabricated at time of publication	Not built at time of publication

CFRP = carbon fiber reinforced polymer; DOT = department of transportation; GFRP = glass fiber reinforced polymer; Unk. = unknown.

[a] Fico et al., 2006; Shing et al., 2003; Zylstra et al, 2001.

[b] Ushijima et al., 2016.

[c] Rohleder et al., 2008.

[d] Rizkalla et al., 1998.

[e] Grace et al., 2004.

[f] American Association of State Highway and Transportation Officials, n.d.

[g] VDOT, 2018.

METHODS

To support the implementation of CFRP reinforcement in piles by VDOT, this study focused on providing assistance in two areas: (1) QA/QC testing for CFRP reinforcement, and (2) options for improving the wedges for anchorage used during the fabrication of CFRP-reinforced precast concrete piles. To accomplish these goals, three tasks were performed:

1. The literature was reviewed.

2. Qualification and validation procedures for CFRP were established.

3. Pretensioning anchorage systems for CFRP piles were reviewed, and a new method of fabrication was proposed.

Task 1: Review of the Literature

Composites, such as FRP, have been used in many industrial environments, including as reinforcement in concrete, but the CFRP material being used in this application, i.e., CFCC, is unique in its shape, a seven-wire strand configuration as opposed to the commonly available rods. Therefore, one focus of the literature review was CFCC. In addition, the review focused on tests and standards that guarantee quality FRP materials are procured. This portion of the review included searching ACI, ASTM International (ASTM), the American Association of State Highway and Transportation Officials (AASHTO), and other DOT standards and specifications.

The literature review also incorporated studies that were part of this research project but were published earlier. These studies focused on the durability of CFRP (Tanks et al., 2017a), the kinetics of in-plane shear degradation (Tanks et al., 2017b), and the quality assessment of CFRP using Charpy impact (CI) testing (Tanks et al., 2016).

Task 2: Establishment of Qualification and Validation Procedures for CFRP

CFRP Durability Testing

For CFRP durability testing, using a digital balance with a precision of 0.1 mg, the mass gain (MG) of the test samples was determined. A heat-flux differential scanning calorimetry (DSC) instrument was also used to perform thermal analysis and measure the glass transition temperature (T_g). Plus, specimens were subjected to uniaxial tensile testing with and without environmental conditioning. A two-stage Fickian model was used to generate moisture sorption predictions.

CI Testing for Quality Assessment

A standard CI tester with 45^{o} tup was used for testing, with a striking velocity of 3 m/s and a maximum impact energy of 330 J. If needed, scanning electron microscopy (SEM) analysis was performed to evaluate the failure surfaces after CI testing.

Chemical Analysis Using Energy Dispersive (X-ray) Spectroscopy

Energy dispersive (x-ray) spectroscopy (EDS) was used in conjunction with SEM for the identification of chemical elements. By generating EDS line or mapping scans, the distribution of various elements can be determined in 1D or 2D, respectively. Thus, the penetration of ions into a composite after exposure to an aqueous solution can be mapped to correlate with the gravimetric moisture sorption measurements. For this study, EDS was performed in conjunction with SEM analysis and used to determine the distribution of chloride-containing salts in the CFRP.

Models for Predicting Residual Strength

Two models were used to describe the observed changes in mechanical properties after exposure to various environmental conditions. One model was proposed by Phani and Bose (1986), hereinafter called the relaxation-based degradation model or the Phani-Bose model, and the other was the moisture-based degradation model. Their respective strengths and weaknesses were compared in terms of simplicity and accuracy. A brief description is provided in this report, but complete details about the mathematical basis for and implementation of both models are provided in Tanks (2015).

Task 3: Review of Pretensioning Anchorage Systems for CFRP Piles and Proposal of a New Method of Fabrication

One of the most significant changes when working with CFRP, other than the strand material, is the anchorage system. This task focused on a review of what has been done in this area and a proposed new method of fabricating custom anchor components that can fit any CFRP material in a relatively inexpensive manner.

Review of Pretensioning Anchorage Systems

A review of the literature was performed to determine other anchorage device options that might be used during the stressing of the CFRP. A survey of current CFRP suppliers was also conducted to determine if other anchoring devices for CFRP were available.

Prototype Design of New Method of Fabricating Pretensioning Anchoring Systems

Design Methodology

Analytical methods were used for calculating approximate required dimensions, and designs were visualized using computer-aided design (CAD) software (.dwg and .iges files for 3D printing). It was also decided that the surface contacting the CFRP strand could be designed to replicate the contour of the strand to ensure maximum surface contact between the wedge and the strand.

Anchor Materials

A standard ASTM A1018 steel was chosen for the barrel because of its strength and stiffness. However, the wedges must carefully conform to the surface of the CFRP and distribute gripping pressure yet remain strong enough to prevent anchorage failure. Materials considered for the wedges included American Iron and Steel Institute (AISI) 303 annealed stainless steel, 6061-T6 aluminum, and poly-ether-ether-ketone (PEEK) thermoplastic reinforced with 30 wt% glass fiber (PEEK-G30). In addition, acrylonitrile-butadiene-styrene was included for 3D printing to model the contours and geometry.

Part Fabrication

Traditional machining methods were used to produce the steel barrel and three wedge prototypes made of AISI 303, 6061-T6, and PEEK-G30. The novel strand-conforming plastic wedges were manufactured by 3D printing, using acrylonitrile-butadiene-styrene stock, from models generated by CAD software.

Anchor Design Testing

To evaluate each prototype, uniaxial tensile testing was conducted using the new anchor design on one end and a clamped-plate anchor serving as a control on the other end. The CFRP specimens were loaded in a steel testing frame with a hydraulic ram at a nominal rate of 10^{-3} in/sec until reaching failure or a predetermined maximum load.

RESULTS AND DISCUSSION

Literature Review

Materials and Specimens

The CFRP evaluated in this study, i.e., CFCC, was manufactured in Japan (Tanks et al., 2017a). CFCC is composed of polyacrylonitrile carbon fibers that are embedded in an amine-cured epoxy matrix. The center wire, or king-wire, from a strand was used for testing. Additional details relating to CFCC are provided in Table 2.

Table 2. Description of CFCC Test Material

Description	Diameter, in (mm)	Fiber	Fiber Volume	Matrix	GUTS, ksi (MPa)
7-wire cable	0.6 (15.2)	PAN	~0.64	Epoxy	338 (2330)
Center wire	0.2 (5.0)			(Amine-cured)	

CFCC = carbon fiber composite cable; GUTS = guaranteed ultimate tensile strength; PAN = polyacrylonitrile.

Guidance on CFRP Testing and Use

Upon review of the literature, it was clear that for FRP materials that are used in concrete, a sizable number of standards are provided by ACI and ASTM. ACI provides guidance on bond testing, pull-out testing, and beam-end testing. ASTM provides guidance on fiber content, creep rupture testing, creep testing, and resistance to alkaline environment. Neither of these organizations provides guidance on determining the weight per foot for FRP materials.

For highway structures, some DOTs are implementing the use of CFRP in some applications in piles and/or beams. Several DOTs have provided guidance with regard to CFRP used in piles (Florida DOT, 2019; VDOT, 2019), and others have focused on beams (American Association of State Highway and Transportation Officials, n.d.).

Exposure Testing

For the three studies by Tanks et al. (Tanks et al., 2016; Tanks et al., 2017a; Tanks et al., 2017b) that incorporated long-term exposure testing, testing was performed on CFRP samples using one of two solutions: (1) a calcium hydroxide solution ($Ca(OH)_2$), hereinafter "CPS," was used to expose the CFRP to a high pH aqueous environment, and (2) a solution made of $Ca(OH)_2$ combined with sodium chloride (NaCl), hereinafter "CPSSW." In addition, four different exposure temperatures and two different pre-loading levels were used for comparisons. All of these different conditions were then monitored, and the results were published in three different studies. The studies were titled as follows:

1. Durability of CFRP Cable Exposed to Simulated Concrete Environments (Tanks et al., 2017a)

2. Kinetics of In-Plane Shear Degradation in Carbon/Epoxy Rods From Exposure to Alkaline and Saline Environments (Tanks et al., 2017b)

3. Charpy Impact Testing to Assess the Quality and Durability of Unidirectional CFRP Rods (Tanks et al., 2016).

Since temperature is a major factor in the various degradation mechanisms common to FRP, temperature can be used to accelerate aging. For testing, the two solutions were poured into either PVC containers or glass beakers (depending on specimen type) and maintained at four temperatures: 20 ^{o}C (68 ^{o}F), 40 ^{o}C (104 ^{o}F), 60 ^{o}C (140 ^{o}F), and 80 ^{o}C (176 ^{o}F). In this report and in the other works by Tanks et al., the Celsius values are referenced since Celsius is commonly used for laboratory measurements and is the base unit of temperature in the metric system. In addition to the environmental conditions mentioned, the effect of tensile stress in

prestressed CFRP was incorporated into the treatment for some CPS environments at 20 °C and 60 °C. Therefore, because of the convenience and potential significance of accelerated durability testing with pre-loading compared to sustained loading, this approach was adopted for 75% ultimate tensile strength (UTS) of the CFCC.

The test matrix for studying the durability of CFRP that was discussed in the studies by Tanks et al. is given in Table 3 (Tanks et al., 2017a). This table also includes additional testing that was done, EDS, and although it was not included in these studies, it is included in this report. Each test method is listed according to the selected environments for that type of test. However, it is important to note that several tests were performed after specific samples were subjected to pre-loading. Table 4 summarizes the pre-loading conditions studied, showing the combinations of solution, temperature, and pre-loading.

Table 3. Test Matrix for Durability of CFRP

Condition	Temperature (°C)	20		40	60		80	
	Medium	CPS	CPSSW	CPS	CPS	CPSSW	CPS	CPSSW
Material Characterization	Mass gain	X	X	X	X	X	X	X
	Uniaxial tensile testing	X	X	-	X	X	-	-
	Short-beam shear testing	X	X	-	X	X	-	-
	Charpy impact testing	X	X	-	X	X	-	-
	Energy dispersive (x-ray) spectroscopy	X	X	-	X	X	-	-
	Differential scanning calorimetry	X	X	-	X	X	-	-
	Scanning electron microscopy	X	X	-	X	X	-	-

CFRP = carbon fiber reinforced polymer; CPS = calcium hydroxide solution; CPSSW = calcium hydroxide plus sodium hydroxide solution.

Table 4. Summary of Combined Environmental Conditions for Studying Durability of CFCC

Temperature (°C)		20		40		60		80	
Medium		CPS	CPSSW	CPS	CPSSW	CPS	CPSSW	CPS	CPSSW
Pre-load	0% UTS	X	X	X	X	X	X	X	X
	75% UTS	X	-	-	-	X	-	-	-

CFCC = carbon fiber composite cable; CPS = calcium hydroxide solution; CPSSW = calcium hydroxide plus sodium hydroxide solution; UTS = ultimate tensile strength.

Durability of CFRP (Tanks et al., 2017a)

Although FRPs can exhibit remarkable mechanical behaviors and provide a lightweight alterative to steel in many structural applications, these material properties can degrade when exposed to certain environmental and load conditions. With CFRP, the polymer matrix is generally susceptible to degradation when exposed to adverse conditions. Therefore, testing that

characterizes changes in durability when CFRP is exposed to different temperatures, alkaline environments, and loading conditions is of value to the engineer who will be embedding CFRP reinforcement in concrete. This study used several techniques to evaluate CFRP that has been exposed to aggressive conditions with the potential to degrade the material (Tanks et al., 2017a).

Using a digital balance with a precision of 0.1 mg, the MG of the test samples was determined. A heat-flux DSC instrument was also used to perform thermal analysis and measure the glass transition temperature (T_g). To observe degradation and other changes in morphology qualitatively, microstructural analysis was conducted using SEM. Specimens were subjected to uniaxial tensile testing with and without environmental conditioning. The uniaxial tensile testing machine was also used to perform short-beam shear (SBS) testing (Tanks et al., 2017).

Based on the MG testing, stress-induced exposure, pre-loading to 75% UTS, resulted in a greater moisture uptake and saturation value when compared to increasing temperature. Although increasing temperature was not as influential as pre-loading, however, it too increased the moisture uptake and saturation values. Moisture penetration was also evident based on DSC measurements, which exhibited a depression in the T_g because of plasticization of the epoxy matrix. However, although uniaxial tensile loading influenced moisture uptake, it was concluded in this work that significant losses are not expected, with this work showing a decrease of less than 4% after 2,000 hours of exposure. It was also highlighted that although more work is needed, the Phani-Bose model showed favorable results for predicting the residual strength of CFRP. Finally, the SBS test demonstrated greater sensitivity to environmental exposure than the tensile test since the matrix and matrix/interface were more affected by the exposure conditions (Tanks et al., 2017).

Kinetics of In-Plane Shear Degradation in Carbon/Epoxy Rods (Tanks et al., 2017b)

Shear strength is another value that can be sensitive to the environment that surrounds the CFRP. Similar to the previous study, MG, DSC, SEM, and SBS testing was used to evaluate the intralaminar shear strength (ILSS) of the CFRP. In addition, acoustic emission monitoring was used to capture the release of acoustic energy during SBS testing.

The study highlighted the influence of the synthetic yarn that is wrapped around the outer circumference of the CFCC to protect the CFRP from abrasion and UV radiation. Although the yarn does not change the axial tensile properties of the wire, it does impose transverse confinement that influences the intralaminar shear behavior measured via SBS testing. The actual ILSS, or the peak stress at the end of the linear portion of the force-displacement curve, is 6.8% greater for CFCC with the yarn wrapping. The apparent stiffness for wrapped CFCC is 13% lower, which is most likely because the measured deflection is a combination of actual specimen displacement and through-thickness compression of the wrapping itself. The most significant effect from the yarn wrapping is the arrested delamination observed after the ILSS peak compared to the progressive delamination of the unwrapped specimens. In fact, the wrapped CFCC continues to carry increasing applied force as the yarn begins to resist delamination through hoop stresses.

The implications of this are twofold: (1) CFCC has greater resistance to shear with the yarn wrapping, which is beneficial for in-service performance; and (2) CFCC specimens should be unwrapped for SBS testing in order to reflect degradation caused by environmental exposure accurately, which is the intended purpose of the test. Therefore, all subsequent specimens were unwrapped to measure ILSS with SBS testing.

The overall intralaminar shear behavior and failure mode of the SBS specimens remained the same for all environmental conditions and exposure durations shown in Figure 3 in the current report using 1,500 hours of exposure as an example. This denotes a similar degradation process among all the conditions in this study since a change in failure mode and progression might suggest the presence of an environmental effect that is unseen from ILSS values alone. On a related note, the full force-displacement curves in Figure 3 in the current report provide information about the delamination-dominant failure mode in the study by Tanks et al. (2017b). After the peak ILSS is reached, additional inelastic energy is dissipated through delamination-based fracture as resistance to applied force decays.

Upon closer inspection of the decaying portion of the curves, it was observed that the numerous sharp drops in force were the result of progressive delamination: each drop corresponded to a new delamination site. Thus, the specimen delaminated into two halves at the neutral axis upon reaching the ILSS, after which both halves behaved as individual short beams and additional delamination occurred to create four sections; this continued until the midspan deflection was large enough to make further delamination difficult by changing the stress state. By comparing the general shape of the curves of exposed specimens in Figure 3 in the current report to control specimens in the study by Tanks et al. (2017b), there seemed to be a more gradual peak at the ILSS, rather than a sharp drop. This seems to point toward plasticization of the epoxy, resulting in less brittle behavior.

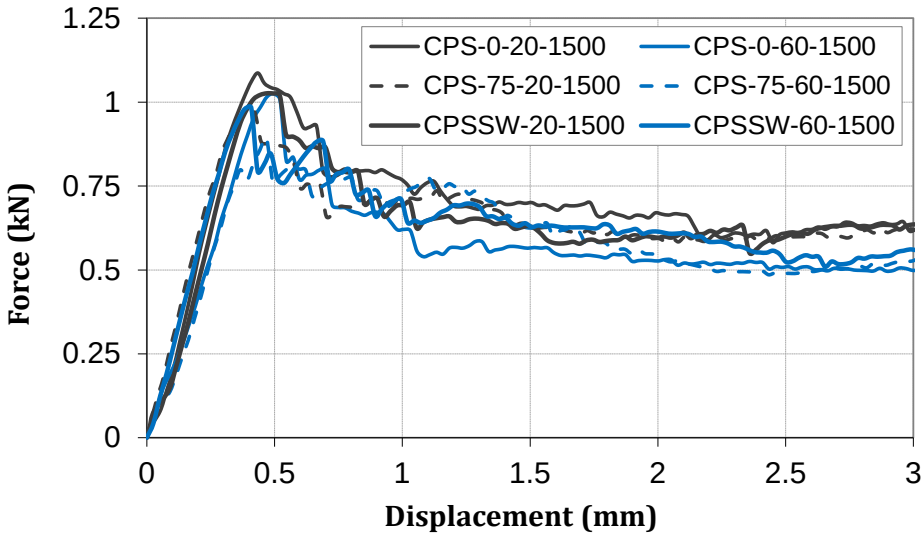

Figure 3. Intralaminar Shear Behavior of CFCC Wires After 1,500 Hours of Exposure. CFCC = carbon fiber composite cable.

The results of SBS testing are listed in Table 5 for all environmental conditions in this study after 500; 1,500; and 2,000 hours of exposure. The residual ILSS is also shown visually with respect to time in the report by Tanks et al. (2017b) and with respect to moisture content in Figure 4 in the current report. There was a distinct trend in ILSS for all environmental conditions wherein a rapid loss happened sometime in the first 500 hours, after which the decrease was much more gradual. Similar to the tensile properties, the ILSS at corresponding moisture contents for different environments overlapped to some degree. Once again, the pre-loaded specimens tended to overlap into a profile separate from the other specimens, showing greater losses because of the morphological changes caused by pre-loading. However, unlike the tensile properties, the ILSS suffered much more from even the mild environments and showed losses up to 18% for the severe case (CPS-75-60). Thus, the sensitivity of the ILSS to environmental effects supports the prominent use of the SBS test as a central component of durability testing programs for FRP composites.

Intralaminar shear strength is controlled by matrix and interfacial failure, which means matrix plasticization or cracking and interfacial debonding are responsible for reduction in the ILSS. An example of a typical fracture surface after SBS testing was captured in several pictures using SEM, with clear debonding in areas with smooth fiber surfaces and some matrix shear failure manifested by the jagged areas, called hackles. If the interface was less affected by the environment, matrix shear would be the principal failure mechanism in SBS testing and there would be more hackles with less fiber surface area exposed. The study by Tanks et al. (2017b) showed a combination of interfacial and matrix failure, but interfacial debonding was more prominent.

Table 5. Summary of ILSS From SBS Testing for Control and Exposed CFCC Specimens

Exposure Condition	Exposure Duration (hr)	ILSS		
		Average (MPa)	COV (%)	Residual (%)
Control (0% UTS)	0	38.40	2.8	100
Control (75% UTS)	0	36.57	3.4	95.24
CPS-0-20	500	37.41	1.8	97.43
	1,500	37.19	2.3	96.85
	2,000	37.16	2.5	96.77
CPS-0-60	500	35.83	3.1	93.31
	1,500	35.17	1.4	91.59
	2,000	34.78	2.2	90.58
CPS-75-20	500	31.61	1.9	90.76
	1,500	31.27	2.8	89.79
	2,000	30.84	4.7	88.55
CPS-75-60	500	29.81	4.0	85.58
	1,500	28.95	2.9	83.13
	2,000	28.74	4.2	82.52
CPSSW-0-20	500	36.85	1.8	95.98
	1,500	36.23	1.8	94.37
	2,000	36.08	2.2	93.95
CPSSW-0-60	500	35.17	2.5	91.58
	1,500	34.27	1.3	89.25
	2,000	33.81	3.7	88.04

ILSS = intralaminar shear strength; SBS = short-beam shear; CFCC = carbon fiber composite cable; COV = coefficient of variation; UTS = ultimate tensile strength; CPS = calcium hydroxide solution; CPSSW = calcium hydroxide plus sodium hydroxide solution.

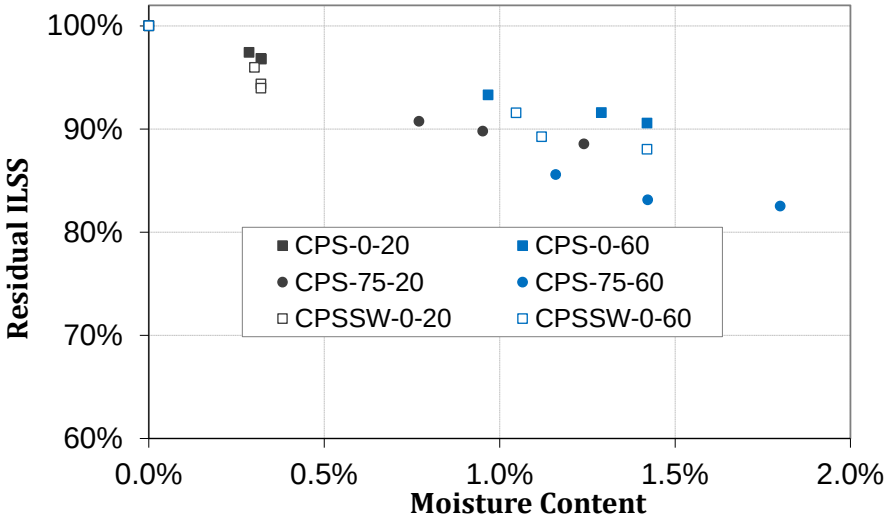

Figure 4. Residual ILSS After 500; 1,500; and 2,000 Hours of Exposure: Strength at Corresponding Moisture Content. ILSS = intralaminar shear strength; CPS = calcium hydroxide solution; CPSSW = calcium hydroxide plus sodium hydroxide solution.

Quality Assessment Using Charpy Impact Testing (Tanks et al., 2016)

Using a standard CI tester with 45^{o} tup and having a striking velocity of 3 m/s and a maximum impact energy of 330 J, this test was performed on specimens within 1 hour of removal from immersion. SEM analysis was then performed to evaluate the failure surfaces after impact testing.

This study acknowledges that although CI, or impact toughness, has very little value as a material property for CFRP in prestressed concrete design, it suggests that impact toughness can be used as a relative value to measure changes after environmental exposure. This study demonstrates that a correlation between the CI and ILSS residuals (using SBS testing) is reasonable, indicating an R^2 value of 0.93 when a linear fit is used. However, it also cautions that the CI test is sensitive to specimen geometry, with size, shape, and notch configuration given as examples.

CFRP Durability Testing

It was highlighted in the earlier study by Tanks et al. that additional research was needed in this area (Tanks et al., 2017a). Therefore, moisture sorption profiles were compiled for the CFCC wires for all environmental conditions listed in the “mass gain” row of Table 3. Mass change was also measured for baseline specimens exposed to air at 60 ^{o}C and 80 ^{o}C in order to determine the true initial moisture content, i.e., the way CFCC would be delivered from the manufacturer. It was found to be 0.065% based on the identical mass loss for both temperatures up to 45 hours; after this point, mass loss comes from excess volatiles and fillers in the matrix and reached equilibrium after 500 hours of exposure time. Within the duration studied here,

there was no observed mass loss that would indicate chemical or thermal breakdown of the epoxy.

As discussed previously, a two-stage Fickian model was used to generate moisture sorption predictions. The thickness *h* in Equation 1 is substituted with the diameter *d* = 5 mm of a CFCC center wire. The difference between a plate specimen with thickness *h* (for which the equation is derived) and a long rod with diameter *d* is likely to be negligible. In a wide plate such as that shown in Figure 5(b), moisture can effectively penetrate in the thickness direction only because of the "restraint" provided by the vast width of the plate; an infinitesimal slice of the plate at an arbitrary location would have the same sorption as any other slice. The long rod shown in Figure 5(a) can also be thought of as infinitesimal slices arranged in a circular pattern, with thickness *d* the same as *h*, and the restraint provided by adjacent slices would still restrict moisture penetration to a single direction. Thus, this substitution in Equation 1 remains valid.

$$M(t) = M_{\infty}\left(1 + k\sqrt{t}\right)\left(1 - \exp\left[-7.3\left\{\frac{Dt}{h^2}\right\}^{0.75}\right]\right) \qquad \text{[Eq. 1]}$$

In Equation 1, *D* is the diffusion coefficient, *t* is time, M_{∞} is the equilibrium (saturated) moisture content, and *k* is a parameter that represents molecular relaxation in the polymer and is obtained through curve-fitting.

To view clearly the moisture sorption profiles and to understand the connection between experimental data and theoretical predictions, Figures 6 through 8 are separated into three categories: (1) specimens exposed to CPS without pre-loading (Figure 6); (2) specimens exposed to CPS with pre-loading (Figure 7); and (3) specimens exposed to CPSSW without pre-loading (Figure 8). The black lines are theoretical predictions using the two-stage Fickian-based model, Equation 1, as shown by Tanks et al. (2016), with curve-fit model parameters listed in Table 6; Bao and Yee (2002) provided details on the meaning and determination of these parameters. It may be noted that the time axis is displayed as the square root of immersion time in seconds$^{1/2}$ (instead of hours), since D is usually expressed as mm^2/s.

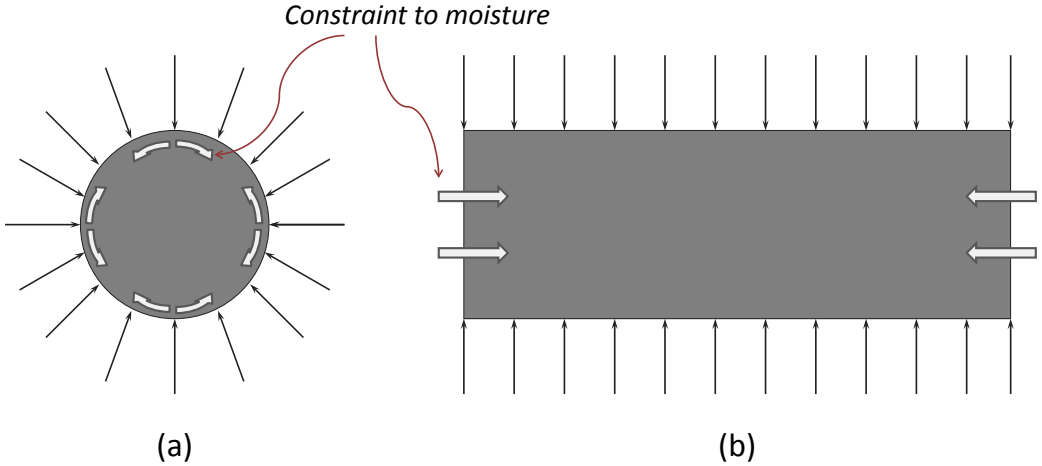

Figure 5. Moisture Penetration for Different Geometries: (a) round rod; (b) infinite flat plate

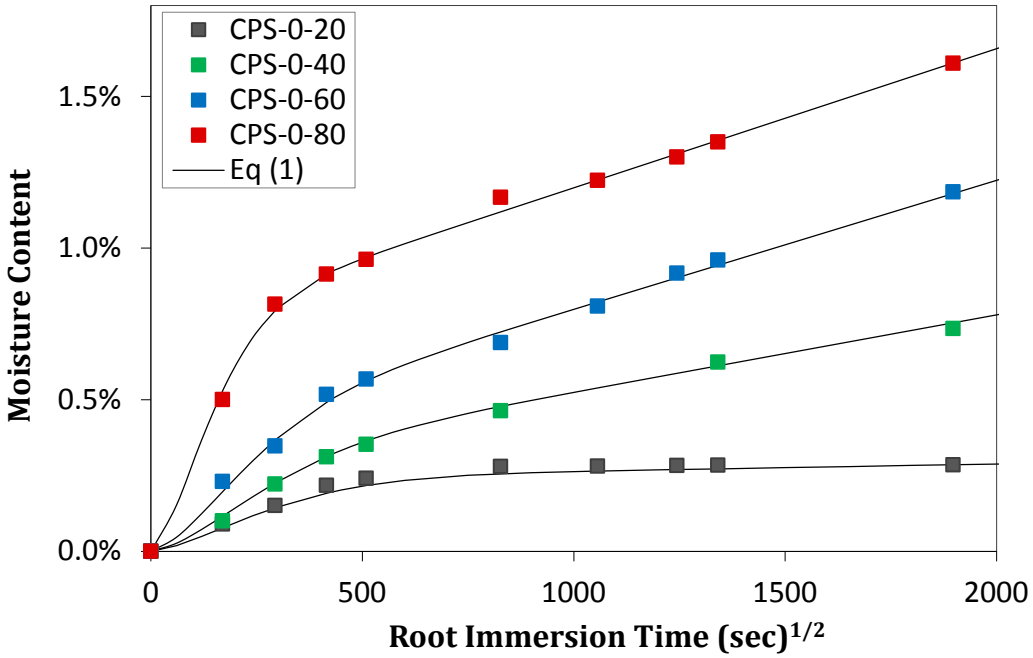

Figure 6. Moisture Sorption Profiles for CPS-0 Environment Data Compared to the Two-Stage Model in Equation 1

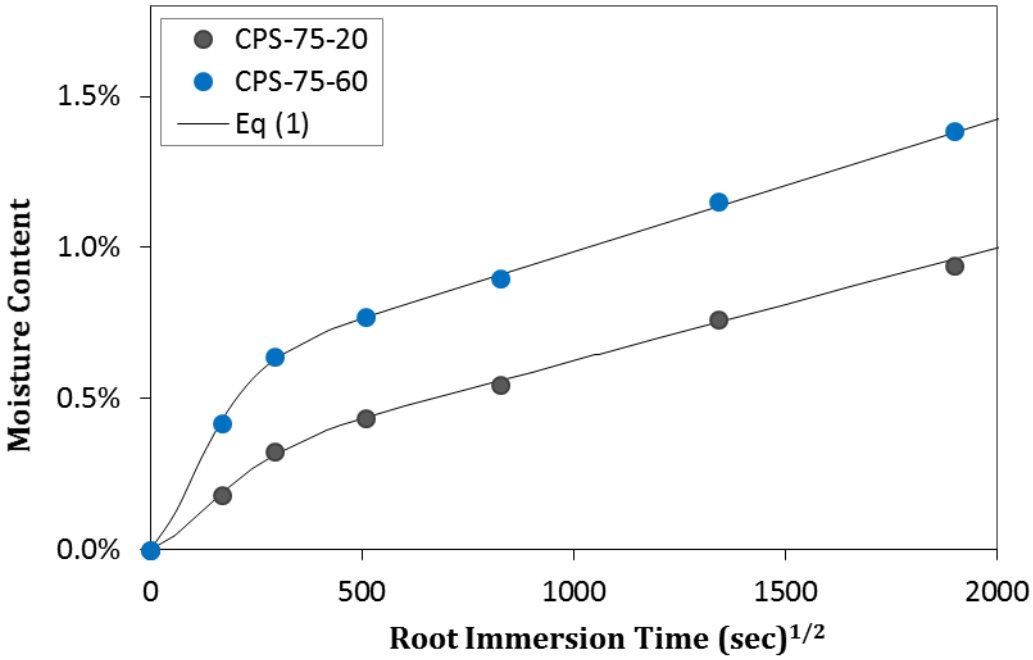

Figure 7. Moisture Sorption Profiles for CPS-75 Environment Data Compared to the Two-Stage Model in Equation 1

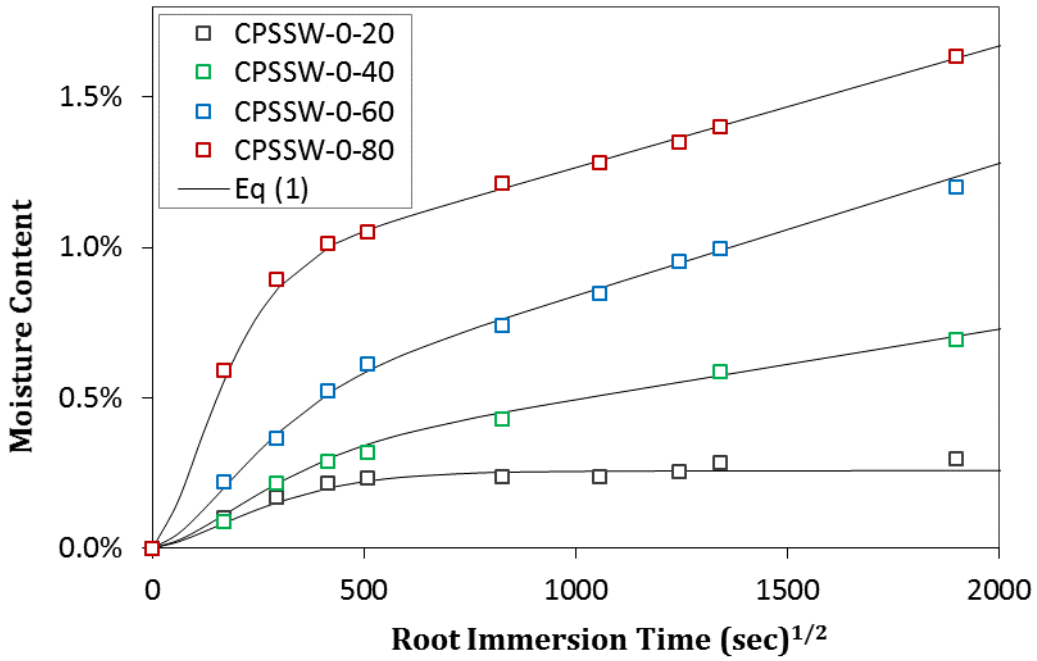

Figure 8. Moisture Sorption Profiles for CPSSW-0 Environment Data Compared to the Two-Stage Model in Equation 1

Table 6. Parameters Used In Two-Stage Moisture Sorption Model for All Exposure Conditions

Parameter	CPS-0				CPS-75		CPSSW-0			
T (^{o}C)	20	40	60	80	20	60	20	40	60	80
M_∞ (%)	0.24	0.27	0.37	0.74	0.25	0.54	0.27	0.24	0.40	0.88
k (10^{-4} $s^{1/2}$)	1.00	9.44	11.40	6.35	15.00	8.00	0.10	9.00	11.00	4.90
D (10^{-4} mm^2/s)	1.7	2.2	3.0	5.0	5.5	7.7	1.9	2.3	2.8	4.5

CPS = calcium hydroxide solution; CPSSW = calcium hydroxide plus sodium hydroxide solution.

This study built on the findings of earlier work that had indicated the benefits of the tensile test, shear test, and glass transition tests. The T_g for control specimens was measured as 109.6 ^{o}C based on the second run. The first run contains a large endothermic peak that starts around 75 ^{o}C before a faint transition; this peak represents some enthalpy recovery from physical aging that occurred from being stored at room temperature between manufacturing and testing. The second run reveals the true T_g, and these features are illustrated in Figure 9.

Results from DSC for all environmental conditions are listed in Table 7 and plotted in Figure 10 with respect to both immersion time and moisture content. It is clear from Figure 10(a) that higher temperature causes a greater rate of depression in T_g for both solutions, yet the influence of pre-loading is unclear—reduction for CPS-75-20 is much greater compared to that for CPS-0-20, and results for CPS-75-60 are much closer to those for CPS-0-60. However, by examining the data in terms of moisture-induced changes in Figure 10(b), a distinct linear relationship becomes clear between T_g and $M(t)$ regardless of temperature, pre-loading, or solution type.

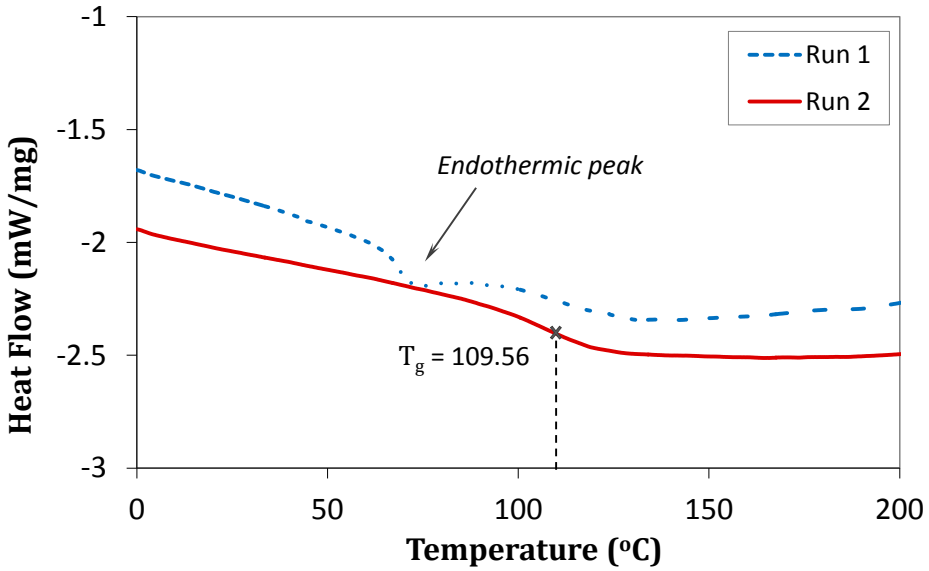

Figure 9. Thermogram From DSC Analysis for CFCC Control Specimens (Using 2 Runs). DSC = differential scanning calorimetry; CFCC = carbon fiber composite cable.

Table 7. Summary of T_g Measured by DSC for Control and Exposed CFCC Specimens

Exposure Duration (hr)	Exposure Condition	T_g (°C)	Exposure Condition	T_g (°C)
0	Control	109.6		
500	CPS-0-20	103.7	CPS-0-60	92.0
1,500		102.1		84.3
2,000		100.9		80.1
500	CPS-75-20	94.6	CPS-75-60	89.0
1,500		89.6		82.2
2,000		83.2		76.9
500	CPSSW-0-20	104.3	CPSSW-0-60	92.7
1,500		101.3		85.8
2,000		100.5		79.1

DSC = differential scanning calorimetry; CFCC = carbon fiber composite cable; CPS = calcium hydroxide solution; CPSSW = calcium hydroxide plus sodium hydroxide solution.

Recalling that the depression mechanism for T_g in thermosetting polymers is the increase in free volume caused by plasticization and relaxation of molecular chains, which are activated by sorbed moisture (Lu et al., 2014; Suh et al., 2001), the validity of the empirical relationship in Figure 10(b) is supported by physical principles. Further, this correlation substantiates the analysis of residual mechanical properties with respect to moisture content, since T_g is an intermediate property that indirectly relates them.

Finally, a summary of the uniaxial tensile testing (triplicate specimens) after exposure durations of 0; 1,500; and 2,000 hours was generated and is provided in Table 8. As long as moisture-induced degradation is the only—or at least, the dominant—active mechanism in causing loss of strength and modulus, a consistent relationship between tensile properties and moisture content should exist. This is especially true for tensile modulus, for which all exposure conditions nearly overlap into a single profile; CPSSW deviates the most compared to the CPS conditions.

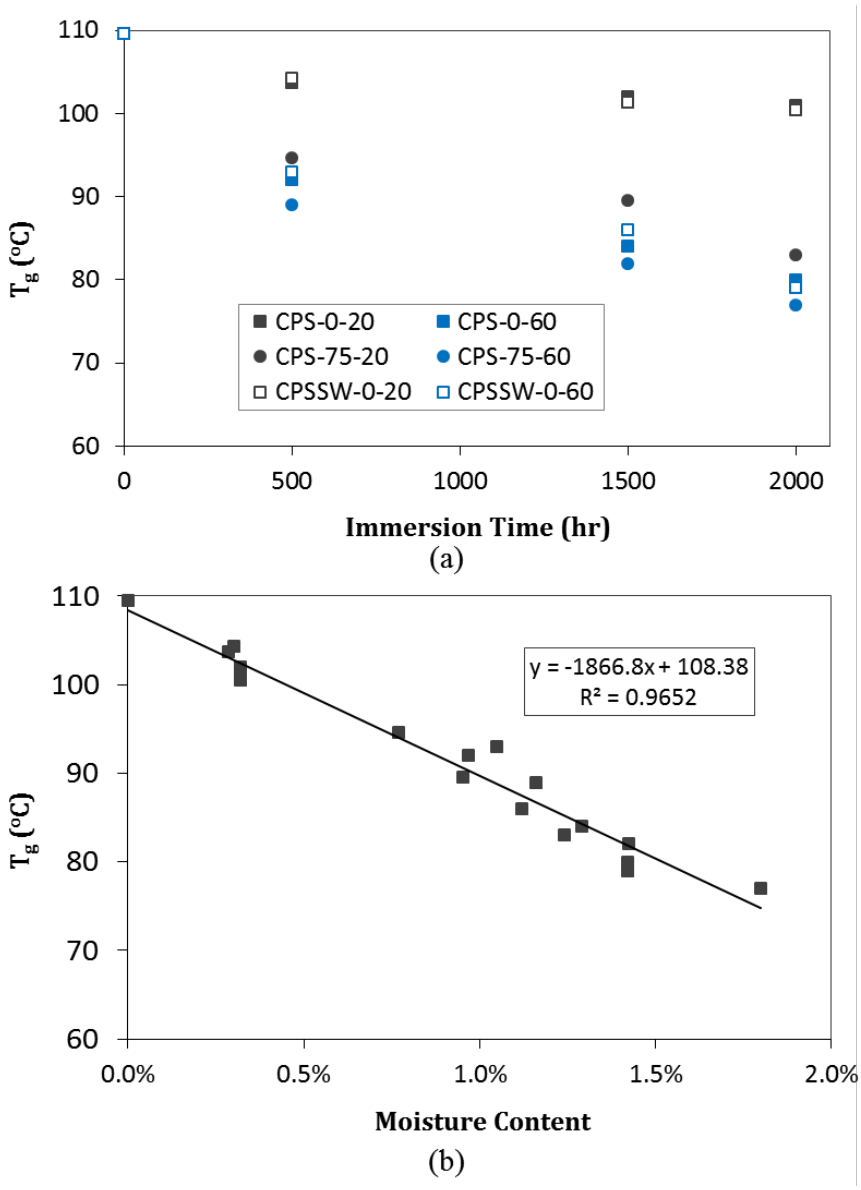

Figure 10. Glass Transition Temperature (T_g) of CFCC After 500; 1,500; and 2,000 Hours of Exposure: (a) T_g over time; (b) T_g at corresponding moisture content

CI Testing for Quality Assessment

As discussed by Tanks et al., CI testing indicates the energy absorption behavior of CFRP under dynamic flexural loading, so it is not always directly related to quasi-static strength (tensile, flexural, or shear) (Tanks et al., 2016). This convenient method was included in the experimental program in order to assess its utility for measuring relative material degradation in a durability testing program. Table 9 contains the results of CI testing using the slotted notch configuration for all environmental conditions after 500; 1,500; and 2,000 hours of immersion. These results are also displayed visually with respect to both time and moisture content in Figures 11 and 12, respectively. As anticipated, the CI data for pre-loaded specimens seem to overlap into a distinguishable profile with respect to $M(t)$, whereas the rest form a separate profile.

Table 8. Summary of Tensile Properties for Control and Exposed CFCC Specimens

Exposure Condition	Exposure Duration (hr)	Tensile Strength			Tensile Modulus		
		Average (MPa)	COV (%)	Residual (%)	Average (GPa)	COV (%)	Residual (%)
Control (0% UTS)	0	3094	2.2	100	150.3	1.3	100
Control (75% UTS)	0	3080	3.2	99.56	149.1	1.6	99.2
CPS-0-20	1,500	3082	2.6	99.62	150.0	1.8	99.80
	2,000	3076	3.1	99.42	149.9	1.9	99.73
CPS-0-60	1,500	3030	4.3	97.95	149.7	2.7	99.60
	2,000	3021	3.5	97.64	149.4	2.0	99.40
CPS-75-20	1,500	3028	4.1	98.32	148.7	3.1	99.73
	2,000	3019	4.7	98.01	148.6	1.9	99.66
CPS-75-60	1,500	2979	4.6	96.71	148.4	2.4	99.50
	2,000	2966	6.2	96.31	148.1	2.2	99.33
CPSSW-0-20	1,500	3079	2.8	99.53	149.9	0.9	99.73
	2,000	3072	2.2	99.29	149.7	2.0	99.63
CPSSW-0-60	1,500	3025	2.7	97.77	149.6	2.8	99.55
	2,000	3012	4.4	97.37	149.3	3.3	99.35

CFCC = carbon fiber composite cable; COV = coefficient of variation; UTS = ultimate tensile strength; CPS = calcium hydroxide solution; CPSSW = calcium hydroxide plus sodium hydroxide solution.

Table 9. Summary of Charpy Impact Test Results for Control and Exposed CFCC Specimens

Exposure Condition	Exposure Duration (hr)	Charpy Impact		
		Average (kJ/m^2)	COV (%)	Residual (%)
Control (0% UTS)	0	661.1	5.5	100
Control (75% UTS)	0	628.0	7.4	95.80
CPS-0-20	500	614.8	4.3	93.08
	1,500	606.2	3.8	91.69
	2,000	602.9	6.5	91.20
CPS-0-60	500	595.0	5.1	90.11
	1,500	577.2	2.4	87.31
	2,000	568.5	5.3	86.02
CPS-75-20	500	556.1	7.7	88.55
	1,500	534.9	4.8	85.16
	2,000	524.4	8.7	83.53
CPS-75-60	500	527.3	6.3	83.96
	1,500	504.5	8.9	80.34
	2,000	506.2	7.0	80.60
CPSSW-0-20	500	612.8	2.8	92.70
	1,500	610.6	5.8	92.37
	2,000	588.4	3.9	89.05
CPSSW-0-60	500	578.4	8.1	87.50
	1,500	566.1	5.3	85.63
	2,000	555.3	5.6	84.00

CFCC = carbon fiber composite cable; COV = coefficient of variation; UTS = ultimate tensile strength; CPS = calcium hydroxide solution; CPSSW = calcium hydroxide plus sodium hydroxide solution.

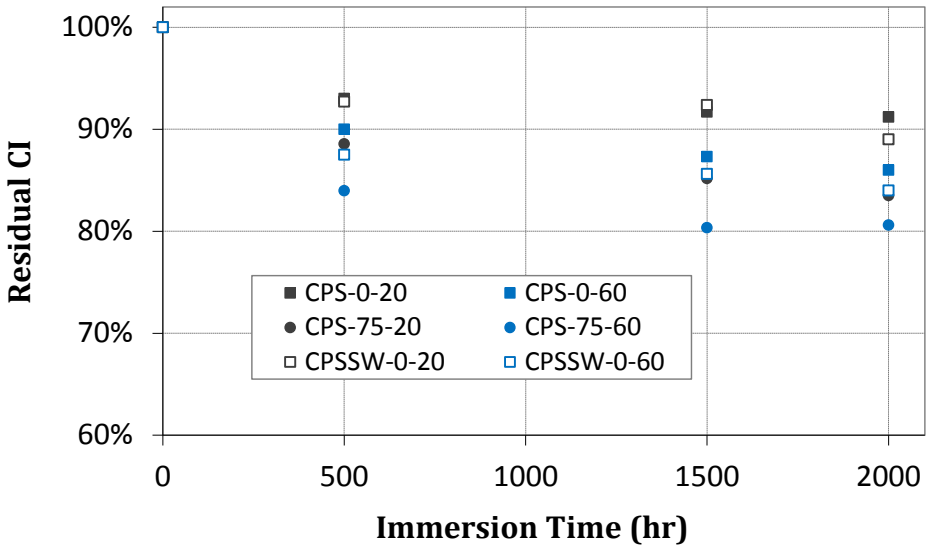

Figure 11. Residual CI Results After 500; 1,500; and 2,000 Hours of Exposure (Percentage Ever Time). CI = Charpy impact; CPS = calcium hydroxide solution; CPSSW = calcium hydroxide plus sodium hydroxide solution.

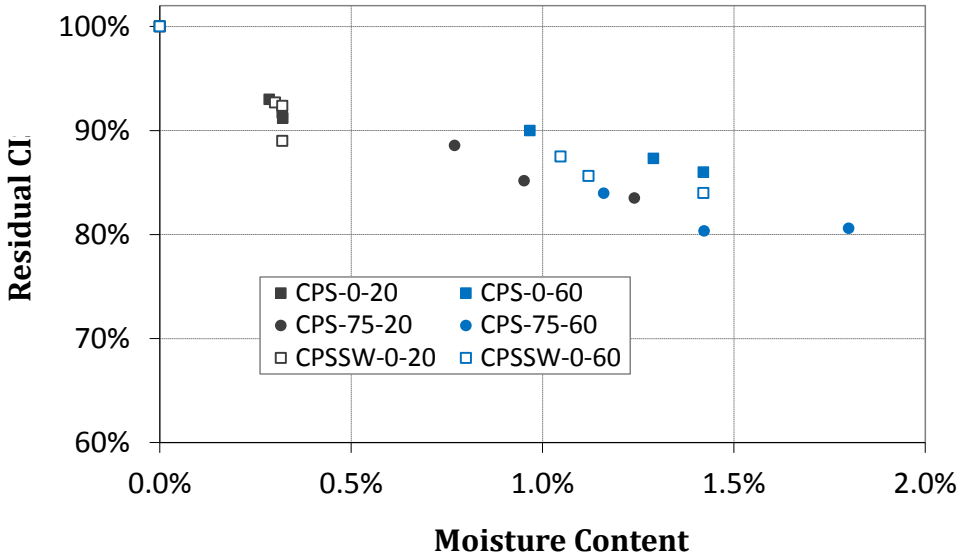

Figure 12. Residual CI Results After 500; 1,500; and 2,000 Hours of Exposure (Percentage at Corresponding Moisture Content Percentages). CI = Charpy impact; CPS = calcium hydroxide solution; CPSSW = calcium hydroxide plus sodium hydroxide solution.

The data followed the same overall trend as ILSS, decreasing sharply until 500 hours and then transitioning to a very gradual state of decay. Another similarity is the notable influence of higher temperature and pre-loading on residual impact behavior, which supports the findings from SBS testing. In fact, the observed losses between the two test methods were of comparable magnitude, and it can be assumed that they provide nearly equivalent information in terms of environmental effects. This close agreement shows that CI testing can be a simple yet useful method for evaluating the environmental durability of FRP composites.

The similar trends between CI and ILSS warranted further analysis to find a meaningful relationship. Three cases were considered regarding the dominant parameter that governs the correlation between CI and ILSS: (1) temperature is dominant, regardless of pre-loading or solution-type; (2) pre-loading is dominant, regardless of temperature or solution type; and (3) solution type is dominant, regardless of temperature or pre-loading. These three cases are shown in Figure 13. Of interest, the relationship between CI and ILSS had the strongest correlation for data grouped by solution type, followed by temperature and pre-loading. Therefore, these results indicate that inferring losses in ILSS because of environmental degradation based on CI data from the same solution type is a reasonable approach.

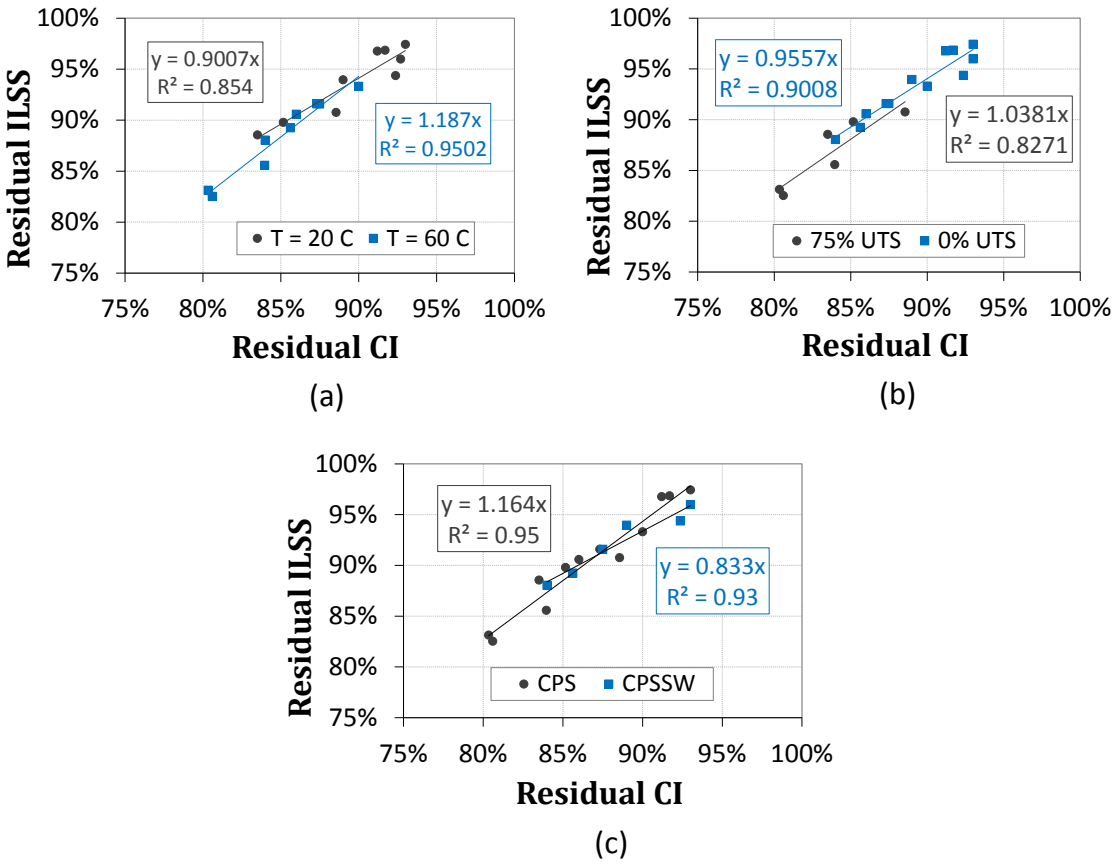

Figure 13. Relationship Between Residual CI test and ILSS Results for Three Environmental Exposure Parameters: (a) temperature; (b) pre-loading; and (c) solution. CI = Charpy impact; ILSS = intralaminar shear strength; CPS = calcium hydroxide solution; CPSSW = calcium hydroxide plus sodium hydroxide solution.

Specimens from all environmental conditions exhibited identical failure modes from CI; flexural failure was caused primarily by fiber pull-out in the tension zone, with the secondary failure mechanism of kink-banding in the compression zone. A typical failed specimen is shown in Figure 14.

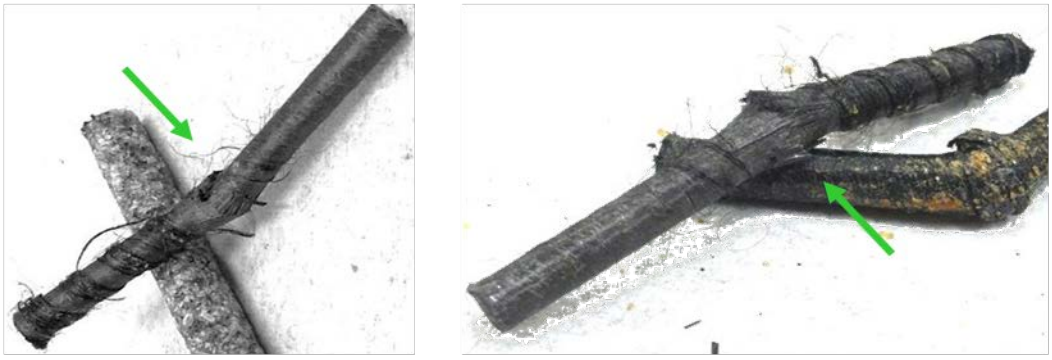

Figure 14. Failed Specimen Showing Both Sides of a CFRP Specimen After CI Testing: left, compression/impact side; right, rotated 180 degress and showing tension/notched side

In addition to exhibiting identical failure modes, specimens from all environments displayed the same microscopic failure mechanisms when viewed with SEM. The degree of fiber pull-out in the tension zone of the fracture surface was so extensive that there is no doubt this was the governing failure mechanism. Fiber pull-out failure is depicted in Figure 15 for a specimen exposed to the CPSSW-0-60 environment. Figure 16 contains images starting from the cross-section and magnifying to the fiber level, showing details of the fracture surface at the tip of the notch, i.e., the extreme tensile surface at the moment of impact. Some small areas of matrix failure are signs that the bond remained intact in localized regions. As the fiber-matrix interface continued to lose integrity over time, the material system's ability to absorb impact energy and to transfer stresses between fibers effectively on a very short time scale was significantly affected. Fractographic analysis using SEM proved effective for visually identifying the failure mechanisms behind the macroscopic failure mode and data that were observed.

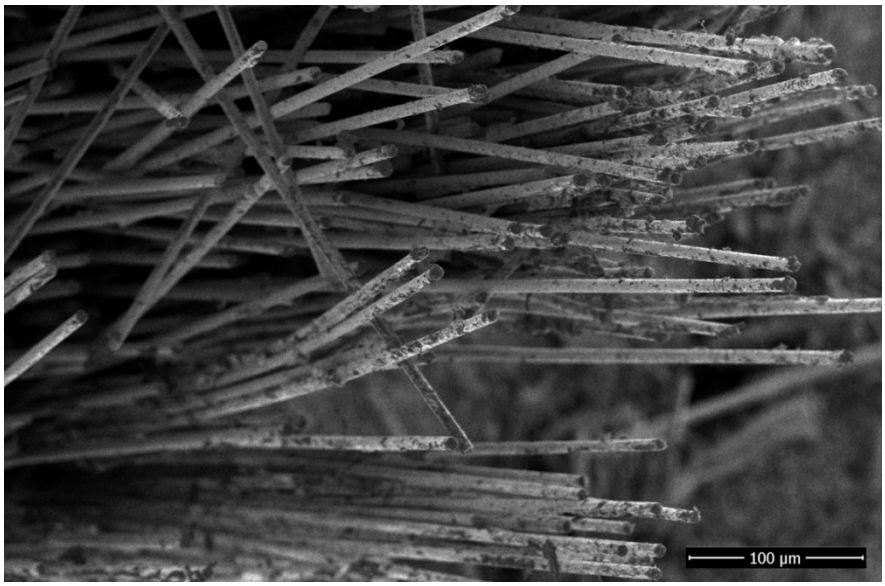

Figure 15. Fracture Surface in Tension Zone Showing Extensive Fiber Pull-Out With Trace Amounts of Epoxy on Fiber Surfaces

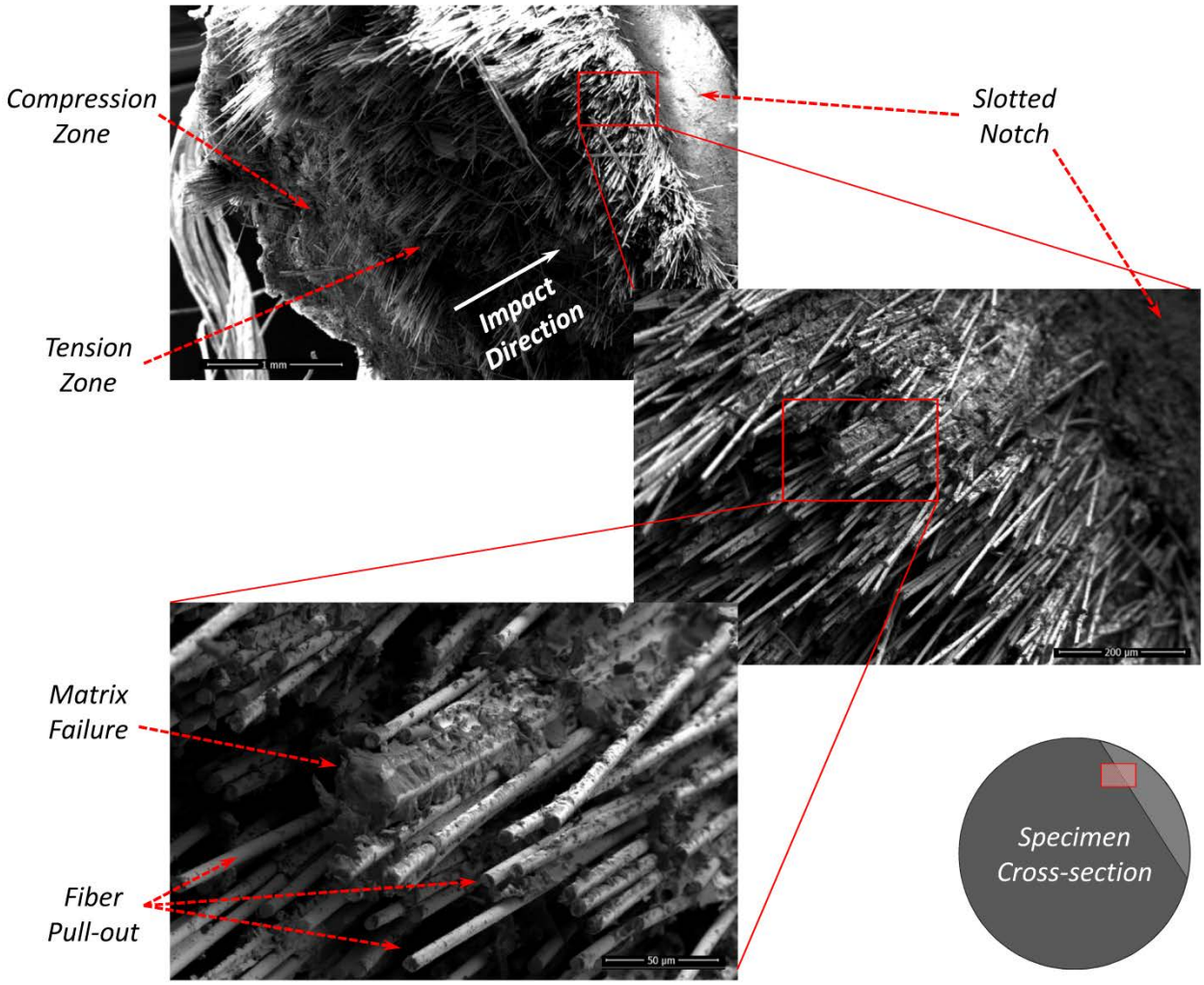

Figure 16. Progressively Microscopic View of Failure Surface in Tension Zone at Notch, Showing Some Matrix Failure Interspersed in Fiber Pull-Out

Chemical Analysis Using EDS

Using the EDS technique in conjunction with SEM was a simple way to investigate the penetration of ions from the CPS and CPSSW solutions based on chemical mapping. This technique is common and very useful for analyzing many materials, both qualitatively and quantitatively. Since Ca^{2+} and Cl^- are the heaviest of the three ions, they were selected as the primary indicators of solution penetration.

Figure 17 demonstrates how 1D linescans can be combined with 2D mapping scans to understand the relative concentration of ions at various locations in the specimen. CPSSW-0-60 was selected as an example for this figure; CPS specimens simply lack Cl^- but contain similar amounts of Ca^{2+} across the surface. A faint color-coded chemical map is overlaid on the SEM micrograph in Figure 17 (left side), showing the relatively high concentrations of Cl^- (blue speckles) in resin-rich areas that are circled in red. This supports the moisture sorption results, and the presence of ions in the CPS/CPSSW solutions actually makes EDS possible: pure water would be detected only by oxygen, which is already present in the CFRP so the signals would be

inconclusive. Finally, results from EDS showed that the ions had penetrated completely through the specimen, which indicates that regardless of whether the material had reached moisture saturation, no discernable moisture gradients existed.

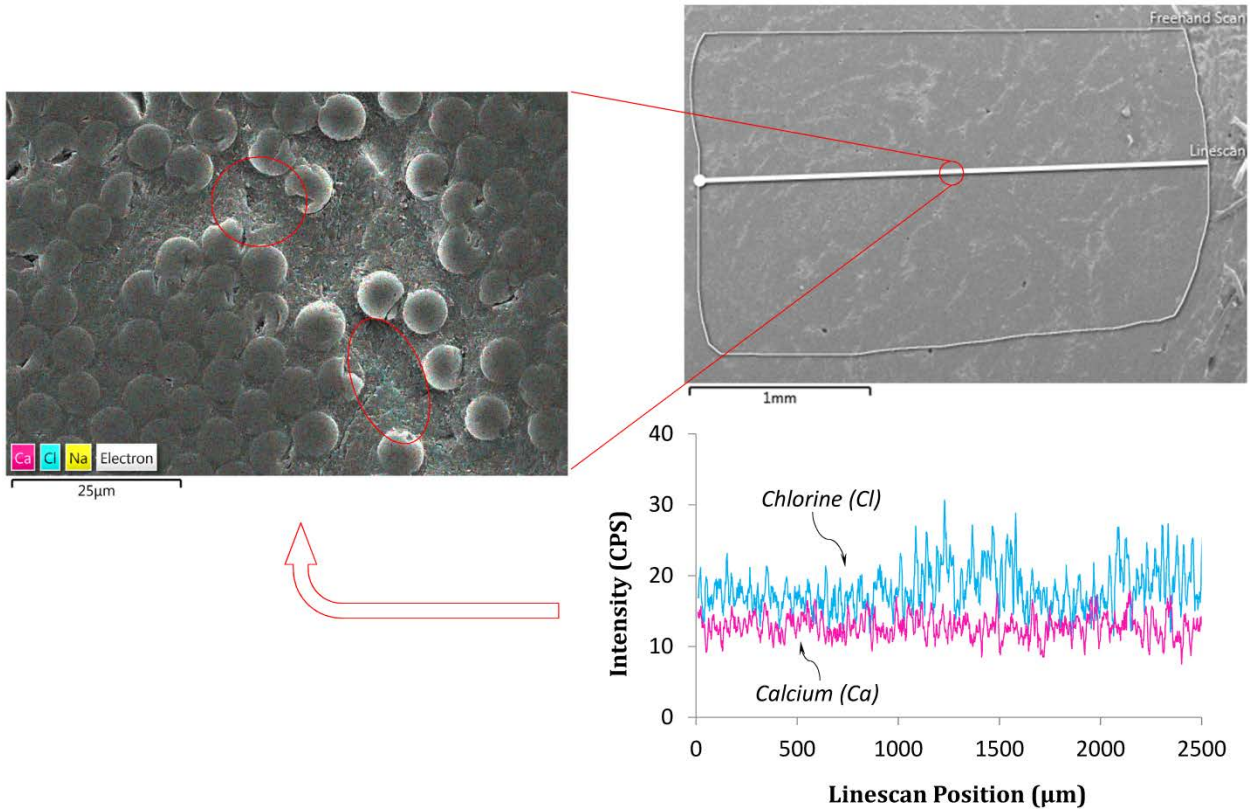

Figure 17. EDS Data From CPSSW-0-60 Specimens After 2,000 Hours of Exposure Showing Combination of 1D and 2D Scans. The higher concentrations of Cl^- are circled in red (left). EDS = energy-dispersive X-ray spectroscopy; CPSSW = calcium hydroxide plus sodium hydroxide solution; CPS = calcium hydroxide solution.

Models for Predicting Residual Strength

Relaxation-Based Degradation Model

Phani and Bose (1986) proposed a model, the relaxation-based degradation model, that invokes viscoelasticity to explain losses in mechanical strength because of environmental degradation. The degradation processes considered were (1) moisture-induced swelling that causes internal stresses, plasticization of the matrix, and deterioration of interfacial bond; and (2) viscoelastic relaxation of this swelling, based on a characteristic relaxation time τ, which depends on temperature (Chen, 2007; Phani and Bose, 1986; Roland, 2008).

$$R_p(t) = R_{p\infty} + (1 + R_{p\infty})e^{-t/\tau} \quad \text{[Eq. 2]}$$

$$\tau(T) = \tau_0 \exp\left(\frac{-E_a}{RT}\right) \quad \text{[Eq. 3]}$$

In Equation 2, $R_p(t)$ is the residual property at time t, $R_{p\infty}$ is the residual property at very large t (approaching infinity), and τ is the characteristic relaxation time for damage to occur. In Equation 3, E_a is the activation energy, R is the universal gas constant, and T is the exposure temperature. It is assumed that unless environmental conditions change, $R_{p\infty}$ is some limit to the loss of the property in question. Thus, this phenomenological model is based loosely on observed physical behavior of glassy polymers but essentially uses a curve-fitting method for the mathematical formulation.

Moisture-Based Degradation Model

Given the correlation observed between residual mechanical properties and moisture content, a new mechanistic model was developed in this study to describe moisture-induced degradation based on free volume theory and polymer physics and calibrated with experimental data.

If moisture-induced degradation is the governing mechanism behind strength reductions in FRP, with negligible chemical reaction kinetics, residual strength can be predicted through a logical progression from moisture sorption to plasticization, from plasticization to softening, and from softening to weakening. The term *softening* is used to describe the thermomechanical behavior when a polymeric material loses stiffness from temperature effects, and *weakening* simply refers to the loss in strength associated with softening. Figure 18 illustrates this progression with a list of key variables that ultimately lead to deteriorated residual strength, with the plasticization and softening processes illustrated in Figure 19. This new model was named the sorption-plasticization-softening-weakening (SPSW) model.

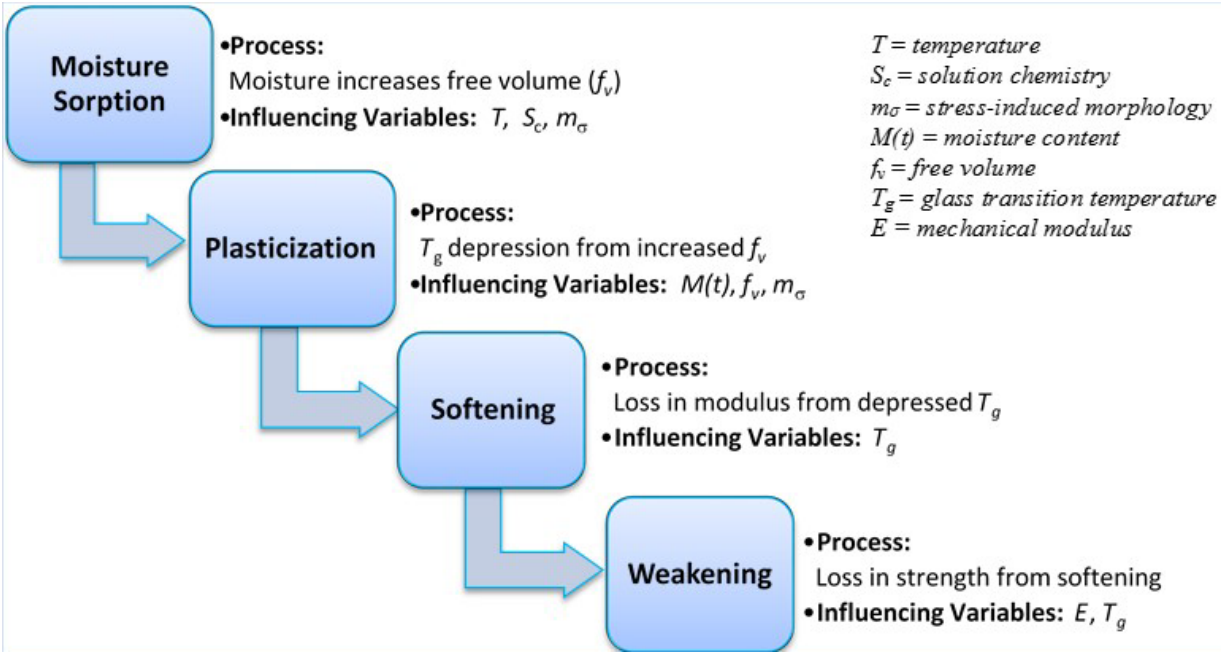

Figure 18. Framework for the Moisture-Based Sorption-Plasticization-Softening-Weakening (SPSW) Model Showing the Progression From Moisture Sorption to Strength Loss

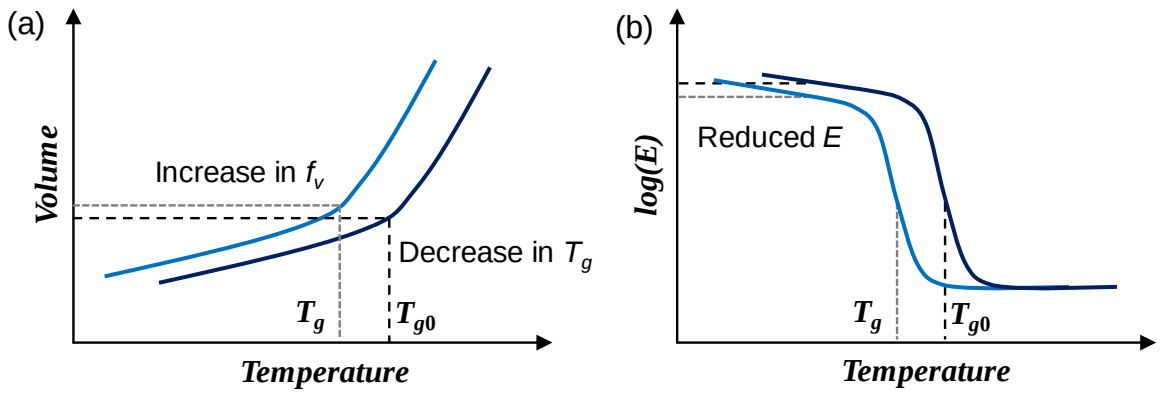

Figure 19. Schematic Representation of Two Main Processes of the Framework of the Sorption-Plasticization-Softening-Weakening Model in Figure 18: (a) plasticization (T_g depression from increase in f_v); (b) softening (stiffness loss from T_g depression). f_v = free volume, T_g = glass transition temperature, and E = elastic modulus.

Prediction Results and Comparisons

The resulting predictions using the relaxation-based model and the moisture-based SPSW model are shown in Figures 20 through 22 for the CPS-0, CPS-75, and CPSSW-0 conditions, respectively. Although predictions for residual ILSS are provided in this report, the predictions for UTS and CI were provided by Tanks (2015).

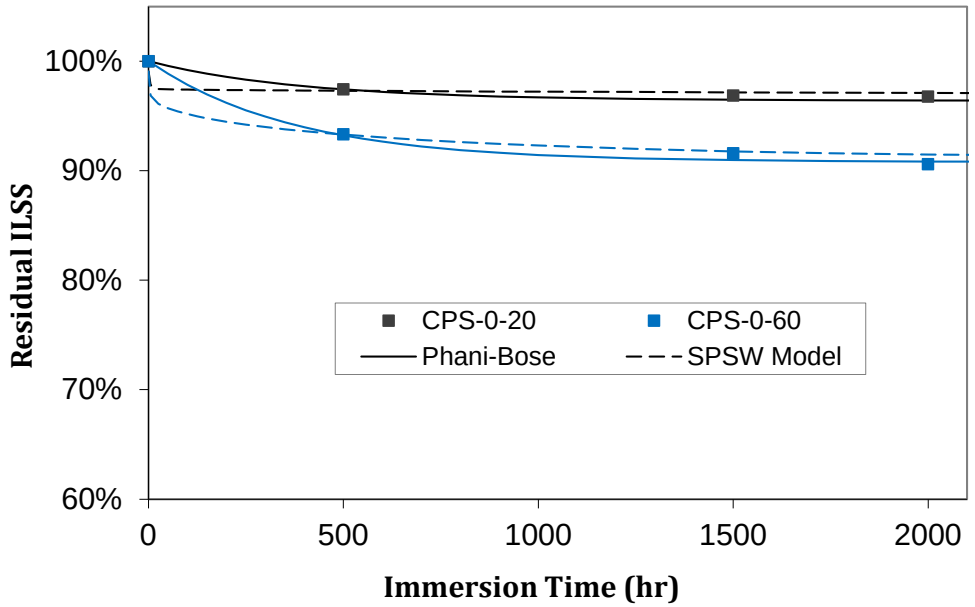

Figure 20. Sorption-Plasticization-Softening-Weakening (SPSW) Model Results for Predicting Residual ILSS for CPS-0 Conditions. ILSS = intralaminar shear strength; CPS = calcium hydroxide solution; Phani-Bose = Phani-Bose Model Curves; SPSW Model = SPSW Model Curves.

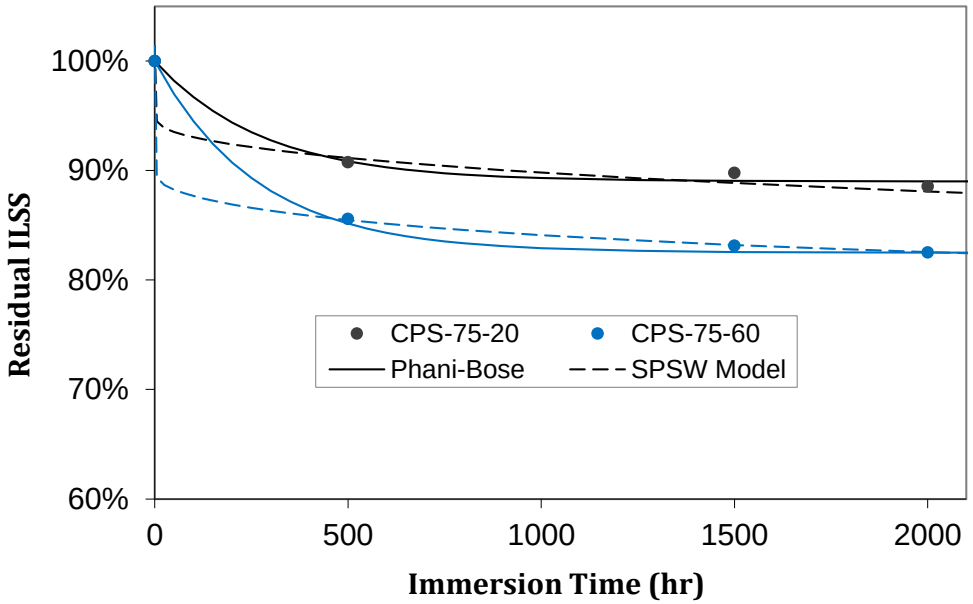

Figure 21. Sorption-Plasticization-Softening-Weakening (SPSW) Model Results for Predicting Residual ILSS for CPS-75 Conditions. ILSS = intralaminar shear strength; CPS = calcium hydroxide solution; Phani-Bose = Phani-Bose Model Curves; SPSW Model = SPSW Model Curves.

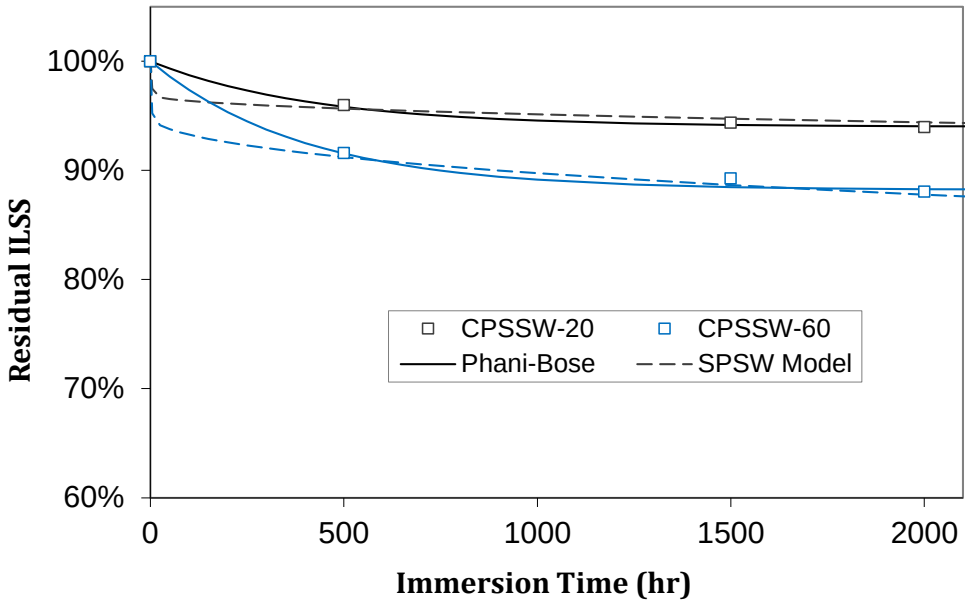

Figure 22. Sorption-Plasticization-Softening-Weakening (SPSW) Model Results for Predicting Residual ILSS for CPSSW-0 Conditions. ILSS = intralaminar shear strength; CPSSW = calcium hydroxide plus sodium hydroxide solution; Phani-Bose = Phani-Bose Model Curves; SPSW Model = SPSW Model Curves.

It is obvious that both models agree with the experimental data very closely. However, there is a major difference in the shape of the decaying portion of the curves at $t < 500$ hours. This is because the Phani-Bose model consists of a purely exponential decay dependent on time alone but the present SPSW model is derived from a combination of exponential and square-root decay dependent on time. More experimental data are needed in the earlier region for immersion

times less than 500 hours. This would provide a more refined determination of the SPSW parameters that could improve the model fit at shorter durations.

In terms of mathematical simplicity, the Phani-Bose model has an advantage over the present model because only two parameters are needed (τ and $R_{p\infty}$), and they are easy to determine using error-minimizing best-fit procedures. The SPSW model essentially requires seven parameters (D, k, M_∞, T_{g0}, a, b, and c). However, it has an advantage over the Phani-Bose model in terms of experimental simplicity, since the process of obtaining these parameters requires fewer types of tests and specimens, relying mostly on thorough characterization of moisture sorption kinetics. For instance, τ and $R_{p\infty}$ for a given property (UTS, ILSS, CI) must be determined for each temperature and solution of interest after several immersion durations. On the other hand, moisture parameters (D, k, M_∞) can be obtained for a range of temperatures and solutions of interest at much shorter immersion durations, and T_{g0} can be measured using DSC; last, the specimens from the moisture sorption tests can be used in mechanical testing to find residual properties and determine a, b, and c.

Finally, aside from simplicity and apparent accuracy, the two models differ in their fundamental basis and formulation. The phenomenological nature of the Phani-Bose model, which is based on damage caused by moisture-induced polymer relaxation, simply assumes a mathematical relationship between two phenomena, and the exponential function describes that well; many processes in polymer materials can be described by exponential functions (Maxwell et al., 2005; Phani and Bose, 1986; Roland, 2008). In addition, the assumption that $R_{p\infty}$ exists, below which the strength will not drop for an indefinite amount of time, is reasonable yet very approximate. By comparison, the SPSW model essentially imposes the same restriction but in the form of moisture saturation (M_∞). Unless conditions change, the moisture content will reach saturation after some time, and since R_p is controlled by T_g, which is controlled by $M(t)$, it logically follows that R_p will remain at a certain value for an indefinite amount of time. Thus, the SPSW model directly incorporates physical and thermomechanical mechanisms to impose a realistic restriction that the Phani-Bose model lacks.

Empirical Models: Comments and Shortcomings

The most basic method for closely modeling the change in mechanical properties over time for a specific environmental condition is to use best-fit linear regression to produce a matching function. Using residual UTS and modulus as an example, data are fit by linear functions of the square root of immersion time (Eq. 4) and immersion time (Eq. 5), respectively:

$$R_{UTS}(t) = a_{UTS}\sqrt{t} + 1 \qquad \text{[Eq. 4]}$$

$$R_{Mod}(t) = a_{Mod}t + 1 \qquad \text{[Eq. 5]}$$

where $R_{UTS}(t)$ and $R_{Mod}(t)$ are the time-dependent residual tensile strength and tensile modulus, respectively; a_{UTS} and a_{Mod} are constants; and t is immersion time. The empirical constant a is essentially the property loss rate, which depends on environmental conditions and can vary widely. As seen in Figure 23, the results from this model agree very well with this data set; however, the model lacks a physical basis for describing degradation and its utility for

characterization or prediction is limited to the data set for which it was constructed. Comparison between environmental conditions requires further analysis of the constant *a*. It is impossible for the residual of a material property to be negative, since the limit is zero, yet Equations 4 and 5 yield negative values when *t* is very large. Thus, the inescapable question is how to determine the valid range of *t* for such simple linear regression models. They can be useful for interpolation within the appropriate data set, rather than extrapolation outside the measured data to make long-term predictions.

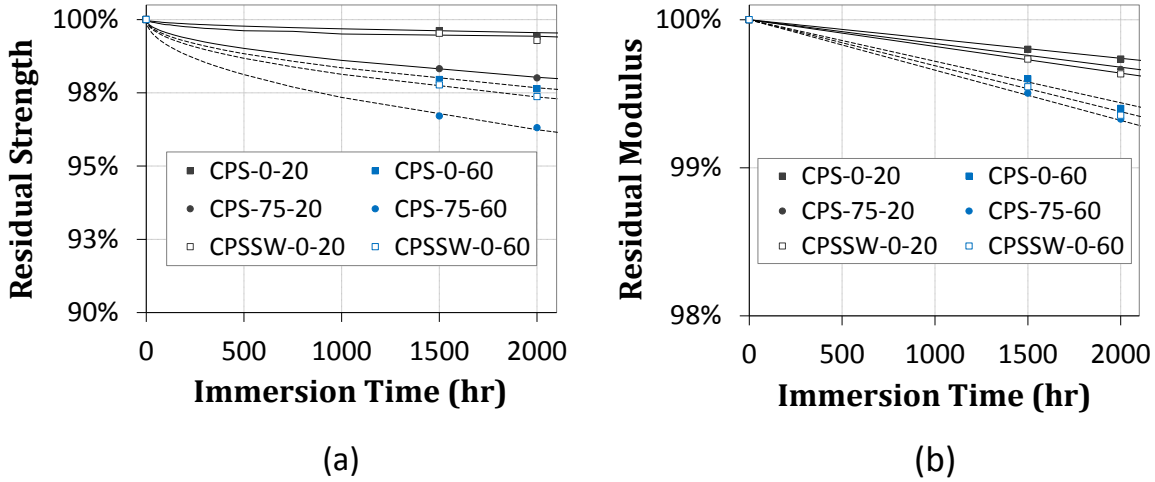

Figure 23. Empirical Models: (a) residual tensile strength; (b) residual tensile modulus. CPS = calcium hydroxide solution; CPSSW = calcium hydroxide plus sodium hydroxide solution.

Summary of Qualification and Validation Procedures for CFRP

An observation from this work was that temperature changes both the sorption rate and saturation level of moisture in CFCC, which is expected from diffusion theory. As temperature increases, the free volume of the polymer matrix also increases, the stiffness of the polymer chains relaxes slightly, and the mobility of excited water molecules rises; these effects lead to the changes in sorption kinetics observed in all three specimen categories as temperature increased. Further, there are significant changes between the CPS-0 and CPS-75 conditions, which can be attributed only to the morphological changes caused by pre-loading. Microcracks, interfacial debonding, change in polymer-free volume, or a combination is likely responsible for these changes.

The experimental program in this study was designed to provide information on two aspects of CFRP durability in a concrete environment: (1) the effects of temperature, alkaline, and alkaline/salt solutions and pre-loading on the mechanical properties of CFCC; and (2) effective techniques and analysis methods for measuring, understanding, and predicting degradation in CFRP. The results indicated that the experimental approach was executed properly, without any major outliers or anomalies, and can be considered a valid methodology for durability testing. Further, a mechanistic model was developed to predict environmental degradation, and it showed excellent agreement with the experimental data.

Gravimetric measurements were successfully used as a simple method for characterizing moisture sorption kinetics for various environmental conditions. A two-stage Fickian model showed good agreement with the experimental data, and moisture sorption kinetics were thermodynamically described using the Arrhenius and van't Hoff equations. The rate of uptake and saturation values increased with higher temperatures, and this effect was identical between the conditions without pre-loading (CPS-0 and CPSSW-0). For specimens pre-loaded to 75% UTS (CPS-75), temperature still influenced the sorption kinetics, but the stress-induced morphological changes showed greater control.

The epoxy matrix showed no signs of chemical degradation via hydrolysis or alkali digestion. Since epoxy lacks ester groups, which are largely responsible for hydrolytic reactions in vinylesters and polyesters, this was expected. The penetration of alkalis and chlorides was even confirmed by chemical analysis using EDS, yet chemical attack did not take place.

Plasticization occurred in the epoxy as a consequence of moisture penetration and was identified through both mechanical testing and thermal analysis. Depression of the glass transition temperature (T_g) was the most obvious sign of plasticization. DSC was a simple, convenient tool for measuring T_g and required very little training or sample preparation.

Uniaxial tensile properties were barely affected after 2.000 hours of immersion, even in the most aggressive environment (CPS-75-60). This makes sense, since these properties are fiber-dominant and the chemically stable carbon fibers do not easily degrade from most environments. Significant losses are not expected without much longer exposure durations or much more severe environmental conditions. However, tensile properties are essential for prestressed concrete design and serviceability, warranting evaluation in this durability testing study.

The epoxy matrix and fiber-matrix interfaces were more susceptible to degradation—for both accelerated and real-time conditions—and the SBS and CI proved to be more effective methods of comparing the effects of environmental conditions. The correlation between SBS and CI results demonstrated that they both capture similar information about the deteriorated condition of CFRP, with similar sensitivities to environmental effects. If the ILSS is not specifically required, CI can be measured instead using the much more convenient CI test.

Microscopic examination of the CFRP using SEM provided a wealth of qualitative data on the material microstructure, condition after exposure, and failure mechanisms after testing. This technique helped explain and support macroscopic observations made through mechanical testing and thermal analysis. Interfacial debonding was found in growing amounts for the six conditions tested, in the following order (lowest to highest): CPS-0-20, CPSSW-0-20, CPS-75-20, CPS-0-60, CPSSW-0-60, and CPS-75-60. In addition, matrix cracking was present in all except CPS-0-20 and CPSSW-0-20 and was most severe in CPS-75-60. Plasticization was responsible for these forms of damage in all specimens, and stress effects were a major cause for pre-loaded CFRP.

Two models were compared for predicting residual strength in CFRP: the relaxation-based degradation model and a moisture-based mechanistic SPSW model developed in this

study. Both models showed excellent agreement with the experimental data available at this time, but thorough validation was not possible without residual strength data from immersion durations less than 500 hours. Although the relaxation-based degradation model is simpler to implement and requires only two parameters, the SPSW model has the advantage of relying on moisture content alone, without the need to account doubly for various temperatures or other environmental effects in the mechanical testing. Moisture sorption is the backbone of the model, and specific, observable physical and thermomechanical mechanisms are represented in the formulation.

Upon completion of this portion of the study, it was clear that some techniques required revision and others required development. Table 10 lists the different techniques that proved beneficial for assessing strand during this study. However, after the current literature was reviewed, several other tests were deemed valuable for evaluating the strand and also the interaction between the concrete and strand. The concrete/strand test is recognized as important because of the need for certain design values. The last four items listed in Table 10 are not currently governed by a standard, but this study has shown how these techniques could be useful in understanding the physical changes in the strand because of long-term exposure to various saltwater and alkaline environments. A more detailed description of the recommended CFRP tests and associated governing standards for acceptance of CFRP materials for use in reinforced concrete is provided in the appendix.

Table 10. Analysis of CFRP and Associated Governing Standards for Acceptance of FRP Materials for Use in Reinforced Concrete

Description	Strand Test		Concrete/ Strand Test	Governing Standard
	Report	Others		
Tensile strength	X		---	ASTM D7205
Tensile modulus of elasticity	X		---	ASTM D7205
Elongation	X		---	ASTM D7205
Bond test	---		X	ACI 440.3R
Glass transition test	X		---	ASTM E1356
Weight per foot	X		---	VTM 139
Fiber content		X	---	ASTM D2584 or ASTM D3171
Creep rupture test		X	---	ASTM D7337
Pull-out test	---		X	ACI 440.3R
Beam-end test	---		X	ACI 440.3R
Creep test		X	---	ASTM D7337
Resistance to alkaline environment	X		---	ASTM D7705
Short-beam shear tests	X			None, developed during study
Charpy impact tests	X			None, developed during study
Chemical analysis using energy dispersive spectroscopy	X		---	None, developed during study
Models for predicting residual strength	X		---	None, additional validation work required

CFRP = carbon fiber reinforced polymer; FRP = fiber reinforced polymer.

Review of Pretensioning Anchorage Systems for CFRP and a Proposed New Method of Fabrication

Review of Pretensioning Anchorage Systems

One of the major challenges of using CFRP prestressing material is creating an anchorage system that fully develops the strength of the tendon without damaging it. Despite the benefits of CFRP prestressing material, the foremost disadvantage is its orthotropic mechanical properties, meaning that the ratio of radial strength to longitudinal strength is low—close to 1:44 (Schmidt et. al., 2012). Using traditional sharp wedge-action anchors made for steel tendons will cause premature fracture of CFRP tendons because of their low radial compressive strength (Dolan et al., 2001). This has resulted in a need to develop an anchorage system that will work with CFRP.

In general, two approaches to anchoring the ends of CFRP have resulted. The first is a modified wedge-barrel assembly that is a variation on the traditional strand-barrel system; however, it often also includes some type of sleeve and possibly longer wedges that help distribute the loading on the strand. The second uses a cementitious material that bonds to the strand and is confined in a rigid cylinder, which is often made of steel. Although both approaches have demonstrated success, they can be slow and are often limited to being applied to a particular strand size and shape. To date, researchers have invented several prominent anchorage designs, most of them patented and licensed to CFRP manufacturers.

The first design discussed used a cold-swaged stainless steel sleeve to protect the tendon, which is then placed in a custom made wedge-barrel assembly that is larger than a traditional one (Pincheira and Woyak, 2001). Although laboratory tests showed that this design could successfully develop the full tensile capacity of the tendon, the authors acknowledged that the process requires special equipment and labor, is time-consuming, and requires a non-traditional assembly.

The FiberLoc design is also a wedge-barrel system that includes a thin-walled aluminum sleeve to protect the tendon, which is then placed in a stainless steel wedge-barrel assembly that is slightly larger than a traditional one (Al-Mayah et al., 2001). The FiberLoc system is licensed to composite manufacturer Pultrall Inc for use with their product.

A unique nonmetallic wedge-barrel assembly made from reactive powder concrete reinforced with CFRP sheets successfully developed full tendon capacity when tested in the laboratory. This assembly is similar in size to a traditional anchorage and passed the Post-Tensioning Institute (PTI) requirements for post-tensioning anchorages (Shaheen and Shrive, 2006). According to the authors, the major drawback is the time and equipment required to make the assembly.

Proposed New Method of Fabrication

All of the initial wedge designs relied on a three-wedge system for making contact between the CFRP and the collet. Figures 24 and 25 show the prototypes developed for straight CFRP rods, and Figure 26 shows the replicated CFRP strand surface.

Figure 24. Anchor Prototypes for Straight CFRP Tendons. CFRP = carbon fiber reinforced polymer.

(a) (b) (c)

Figure 25. Anchor Wedges: (a) PEEK-G30; (b) 6061-T6 aluminum; (c) AISI 303 stainless steel.

Figure 26. Prototype of 3-Piece 3D Printed Wedges for CFCC, Made From ABS Thermoplastic. CFCC = carbon fiber composite cable; ABS = Acrylonitrile-Butadiene-Styrene.

Figure 27. Prototype of Longer 8-in, 2-Piece 3D Printed Wedges for CFCC. CFCC = carbon fiber composite cable.

After the 3D printed three-wedge system was evaluated, it was decided that a simpler 3D printed two-wedge system would be easier to work with. It was also decided that replicating the surface of the CFRP material would also be more challenging to work with in the field. This is because the twist of the CFCC strand would require the wedges to rotate when moving along the strand in order to maintain formfitting contact with the strand surface. With these changes in mind, a new generation of wedge was designed for 3D printing.

The new wedge design would be a two-wedge system that would include longer wedges. The inside surface shape would be hexagonal with texture added to the interior to create friction between the wedges and CFRP. For testing, 4-, 6-, and 8-in designs were generated, with examples of the different lengths shown in Figures 26 through 28. A drawing of one of the 6-in designs that was used to generate the 3D printed wedge, as well as a 3D printed 4-in plastic wedge, is shown in Figure 28.

At the time this report was written, work had begun on fabricating the wedges for testing. Besides the additively manufactured plastic wedges shown, both machined and additively manufactured metal wedges were also produced. Although testing was not possible at the time of publication, the Virginia Transportation Research Council (VTRC) is continuing work on the development of an improved wedge system for CFRP. This wedge would increase production rates during pretensioning and allow for easier use in post-tensioning applications. It is also possible that this wedge design could be used for stainless steel strand post-tensioning applications.

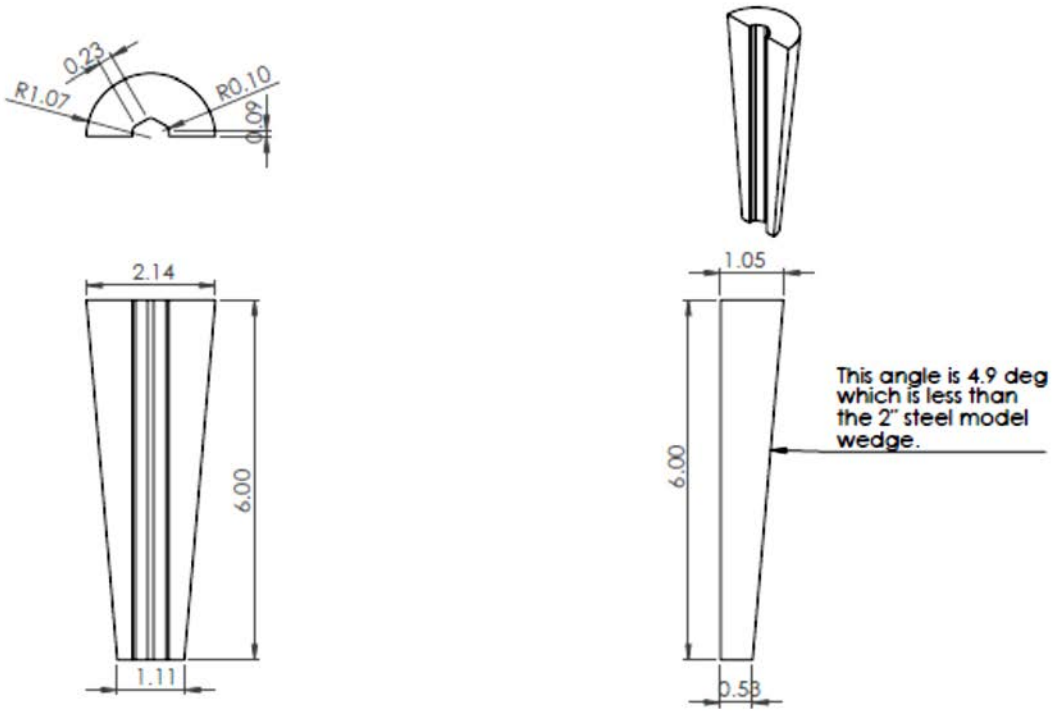

(a)

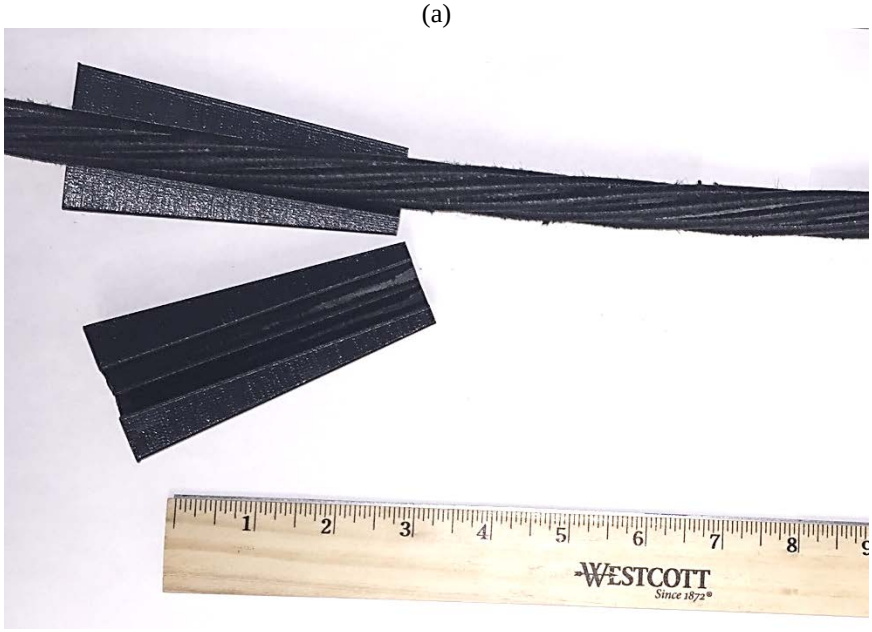

(b)

Figure 28. Examples of Wedges: (a) illustration of a 6-in 2-wedge system that relies on friction between the strand and interior hexagonal wedge surface to maintain a load rather than conventional teeth wedges; (b) 3D printed plastic prototype of the 4-in wedge

CONCLUSIONS

- *Mechanical testing (tensile and shear), chemical analysis, and glass transition temperature testing provide valuable information on the uniformity and quality of CFRP reinforcement; thus, a durable material can be validated with these tests.*

- *Gravimetric analysis characterizes moisture sorption kinetics for various environmental conditions and is a simple method.* The *rate of uptake and saturation values increased with higher temperature and in the presence of pre-loading. Moisture sorption is a measure of the durability of the composite.*

- *The aging process of CFCC reinforcement is slow, such that satisfactory performance is expected. The epoxy matrix showed no signs of chemical degradation, only physical aging through plasticization (softening) after exposure to moisture (i.e., CPS/CPSSW solutions).*

- *DSC is a simple, convenient tool for measuring T_g that requires little training or sample preparation. T_g is a good measure for consistent performance.*

- *SBS and CI tests are effective methods of evaluating the effects of environmental exposure. Higher values indicate improved performance.*

- *Microscopic examination of CFRP using SEM support macroscopic observations made through mechanical testing and thermal analysis.*

- *SEM with EDS provides information on the movement of ions into the composite. Restricted movement leads to better performance.*

- *A promising wedge design has been developed.*

RECOMMENDATIONS

1. *VDOT's Materials Division should prepare guidelines for checking the durability of CFRP reinforcement. The manufacturers should provide data indicating conformance with the guidelines. The guidelines should include the following:*

    - *The SBS test in addition to the uniaxial tensile test should be used. The CI test is also recommended as a convenient supplementary test method for durability evaluation.*

    - *Moisture sorption kinetics should be the central focus of any durability testing program conducted for CFRP materials.*

    - *The use of DSC is recommended for measuring thermal properties of CFRP before and after environmental exposure. This instrument requires little training, and the analysis can be completed quickly.*

- *If the CFRP in question will be used as pretensioning material, the durability testing should include pre-loading at stress levels similar to those expected in the structural element in order to incorporate relevant damage.*

2. *VTRC should continue work on the development of an improved wedge system for CFRP. Such a wedge would increase production rates during pretensioning and allow for easier use in post-tensioning applications. It is also possible that such a wedge could be used for stainless steel strand.*

IMPLEMENTATION AND BENEFITS

Implementation

Recommendation 1 has been implemented. Guidelines were developed for the acceptance and testing of CFRP reinforcement for piles that included the majority of tests assessed in this study. The guidelines include tests to ensure that quality CFRP is used in VDOT projects.

Work for implementing Recommendation 2 is ongoing. To accomplish the goal set forth in Recommendation 2, a new study will be initiated and a recommended wedge system will be provided 3 years after the publication of this report.

Benefits

This study has resulted in tangible benefits to VDOT by ensuring an effective QC program for CFRP strand and future benefits through lower production cost.

With respect to Recommendation 1, CFRP is still a relatively new material for the infrastructure sector, and definitely for VDOT, which means that improved testing methods for material characterization and acceptance and QC are needed for cost-effective implementation. This study contributed valuable information on a robust accelerated durability testing procedure, which can be implemented by VDOT's Materials Division with minimal training or equipment required. Thus, the benefit to VDOT of implementing this recommendation lies in streamlining the material testing approach that is more reliable for accepting and comparing CFRP products.

With respect to Recommendation 2, this study proposed a new approach to manufacturing wedge anchors that could greatly improve fabrication time for CFRP pretensioned concrete beams. These improvements would then equate to cost savings for the purchaser, which could be VDOT.

ACKNOWLEDGMENTS

The authors recognize the contributions of VDOT's Structure and Bridge Division and Materials Division and the Federal Highway Administration for the support they provided during this study. The authors specifically recognize the input and assistance of William Clark, Mark O'Masta, Arthur Ordel, Katherine Rader, Ed Spenceley, Rachel Weeks, and Richard White.

REFERENCES

American Association of State Highway and Transportation Officials. AASHTO Innovation Initiative: Carbon Fiber Reinforced Polymer Strands. n.d. http://aii.transportation.org/Pages/Carbon-Fiber-Reinforced-Polymer-Strands.aspx. Accessed May 17, 2018.

American Concrete Institute, ACI Committee 440. *Accelerated Conditioning Protocols for Durability Assessment of Internal and External Fiber Reinforced Polymer (FRP) Reinforcement for Concrete.* Farmington Hills, MI, 2014.

Al-Mayah, A., Soudki, K.A., and Plumtree, A. Experimental and Analytical Investigation of a Stainless Steel Anchorage for CFRP Prestressing Tendons. *PCI Journal*, Vol. 46, Issue 2, March 2001, pp. 88-100.

Bao, L.-R., and Yee, A. Effect of Temperature on Moisture Absorption in a Bismaleimide Resin and Its Carbon Fiber Composites. *Polymer*, Vol. 43, Issue 14, 2002, pp. 3987-3997.

Chen, Y. *Accelerated Ageing Tests and Long-term Prediction Models for Durability of FRP Bars in Concrete.* West Virginia University Libraries, Morgantown, 2007.

Cox, W.R. Implementation of Flexible Filler for Post-Tensioning Corrosion Protection in Florida. *Aspire—The Concrete Bridge Magazine*, Winter 2017, p. 36.

Dolan, C.W., Bakis, C.E., and Nanni, A. *Design Recommendations for Concrete Structures Prestressed With FRP Tendons.* Federal Highway Administration, Washington, DC, 2001.

Fico, R., Galati, N., Prota, A., and Nanni, A. *Southview Bridge Rehabilitation in Rolla, MO: Volume I: Design and Construction.* U.S. Department of Transportation, Washington, DC, 2006.

Florida Department of Transportation. *Standard Specifications for Road and Bridge Construction.* Tallahassee, 2019.

Grace, N.F., Jensen, E.A., Eamon, C.D., and Shi, X. Life-Cycle Cost Analysis of Carbon Fiber-Reinforced Polymer Reinforced Concrete Bridges. *ACI Structural Journal,* Vol. 109, Issue 5, September 2012, pp. 697-704.

Grace, N.F., Roller, J.J., Navarre, F.C., Nacey, R.B., and Bonus, W. Load Testing a CFRP-Reinforced Bridge. *Concrete International,* Vol. 26, Issue 7, July 2004, pp. 51-57.

Hartt, W.H., and Rapa, M. *Condition Assessment of Jackets Upon Pilings for Florida Bridge Substructures.* Florida Department of Transportation, Tallahassee, 1998.

Lu, Z., Xian, G., and Li, H. Effects of Thermal Aging on the Water Uptake Behavior of Pultruded BFRP Plates. *Polymer Degradation and Stability,* Vol. 110, 2014, pp. 216-224.

Maxwell, A.S., Broughton, W.R., Dean, G., and Sims, G.D. *Review of Accelerated Ageing Methods and Lifetime Prediction Techniques for Polymeric Materials.* NPL Report. DEPC-MPR 016. National Physical Laboratory, Hampton Road, Teddington, Middlesex, UKm March 2005.

Ozyildirim, H.C., and Sharp, S.R. Piles With Corrosion-Free Carbon Fiber Composite Cable in Virginia. *Concrete Bridge Views,* Issue 74, Jan/Feb, 2014.

Phani, K., and Bose, N. Hydrothermal Ageing of CSM-Laminate During Water Immersion: An Acousto-Ultrasonic Study. *Journal of Materials Science,* Vol. 21, Issue 10, 1986, pp. 3633-3637.

Pincheira, J.A., and Woyak, J.P. Anchorage of Carbon Fiber-Reinforced Polymer (CFRP) Tendons Using Cold-Swaged Sleeves. *PCI Journal,* Vol. 46, Issue 6, November-December 2001, pp. 100-111.

Rizkalla, S., Shehata, E., Abdelrahman, A., and Tadros, G. The New Generation (Design and Construction of Highway Bridge). *Concrete International,* Vol. 20, Issue 6, 1998, pp. 35-38.

Rohleder, W., Jr., Tang, B., Doe, T., Grace, N., and Burgess, B. Carbon Fiber-Reinforced Polymer Strand Application on Cable-Stayed Bridge, Penobscot Narrows, Maine. *Transportation Research Record: Journal of the Transportation Research Board,* No. 2050, 2008, pp. 169-176.

Roland, C. Characteristic Relaxation Times and Their Invariance to Thermodynamic Conditions. *Soft Materials,* Vol. 4, Issue 12, 2008, pp. 2316-2322.

Schmidt, J.W., Bennitz, A., Täljsten, B., Goltermann, P., and Pedersen, H. Mechanical Anchorage of FRP Tendons: A Literature Review. *Construction and Building Materials,* Vol. 32, July 2012, pp. 110-121.

Shaheen, E., and Shrive, N. Reactive Powder Concrete Anchorage for Post-Tensioning With Carbon Fiber-Reinforced Polymer Tendons. *ACI Materials Journal*, Vol. 103, Issue 6, November 2006, pp. 436-443.

Sharp, S.R., and Moruza, A.K. *Field Comparison of the Installation and Cost of Placement of Epoxy-Coated and MMFX 2 Steel Deck Reinforcement: Establishing a Baseline for Future Deck Monitoring.* VTRC 09-R9. Virginia Transportation Research Council, Charlottesville, 2009.

Shing, P.B., Borlin, K.A., and Marzahn, G. *Evaluation of a Bridge Deck With CFRP Prestressed Panels Under Fatigue Load Cycles.* CDOT-DTD-R-2003-11. Colorado Department of Transportation, Denver, 2003.

Sprinkel, M.M. VDOT Experience With Grouts and Grouted Post-Tensioned Tendons. *PTI Journal*, Vol. 11, Issue 1, August 2015, pp. 51-61.

Sprinkel, M.M., and Balakumaran, S.S.G. Problems With the Continuous Spliced Post-tensioned Prestressed Concrete Bulb Tee Girder Spans at West Point Virginia. *Transportation Research Record: Journal of the Transportation Research Board*, No. 2642, 2017, pp. 46-54.

Suh, D.-W., Ku, M.-K., Nam, J.-D., Kim, B.-S., and Yoon, S.-C. Equilibrium Water Uptake of Epoxy/Carbon Fiber Composites in Hygrothermal Environmental Conditions. *Journal of Composite Materials*, Vol. 35, No. 3, 2001, pp. 264-278.

Tanks, J.D. *Influence of Temperature and Stress on the Durability of Carbon Fiber Reinforced Polymer (CFRP) Strands in a Concrete Environment.* Department of Civil and Environmental Engineering, University of Virginia, Charlottesville, 2015.

Tanks, J., Sharp, S., and Harris, D. Charpy Impact Testing to Assess the Quality and Durability of Unidirectional CFRP Rods. *Polymer Testing*, Vol. 51, 2016, pp. 63-68.

Tanks, J., Sharp, S., Harris, D., and Ozyildirim, C. Durability of CFRP Cable Exposed to Simulated Concrete Environments. *Advanced Composite Materials*, Vol. 26, Issue 3, 2017a, pp. 245-258.

Tanks, J., Sharp, S., and Harris, D. Kinetics of In-Plane Shear Degradation in Carbon/Epoxy Rods From Exposure to Alkaline and Saline Environments. *Composites Part B*, Vol. 110, 2017b, pp. 204-212.

Ushijima, K., Enomoto, T., Kose, N., and Yamamoto, Y. Field Deployment of Carbon-Fiber-Reinforced Polymer in Bridge Applications. *PCI Journal*, Vol. 61, No. 5, 2016, pp. 29-36

Virginia Department of Transportation. In Design: Laskin Road Bridge Replacement and Widening Project. 2018. http://www.virginiadot.org/projects/hamptonroads/laskin_road.asp. Accessed May 17, 2018.

Virginia Department of Transportation. *Part 2—Chapter 12 / Prestressed and Post-Tensioned Concrete.* 2019. http://www.virginiadot.org/business/resources/bridge/Manuals/Part2/Chapter12.pdf. Accessed April 24, 2019.

Zylstra, R., Shing, P.B., and Xim Y. *Evaluation of FRP Prestressed Panels/Slabs for I-225 / Parker Road Project.* CDOT-DTD-R-2001-14. Colorado Department of Transportation, Denver, 2001.

APPENDIX

RECOMMENDED CFRP TESTS AND ASSOCIATED GOVERNING STANDARDS FOR ACCEPTANCE OF CFRP MATERIALS FOR USE IN REINFORCED CONCRETE BY VDOT

Test Description	Qualification Tests	Verification Tests	Governing Standard
Tensile strength	X	X	ASTM D7205
Tensile modulus of elasticity	X	X	ASTM D7205
Elongation	X	X	ASTM D7205
Bond test	X	X	ACI 440.3R
Glass transition test	X	X	ASTM E1356
Weight per foot	X	X	VTM 139
Fiber content	X	X	ASTM D2584 or ASTM D3171
Creep rupture test	X	---	ASTM D7337
Pull-out test	X	---	ACI 440.3R
Beam-end test	X	---	ACI 440.3R
Creep test	X	---	ASTM D7337
Resistance to alkaline environment	X	---	ASTM D7705

Description of CFRP Tests and Proposed Requirements

Tensile Strength

Scope: Indicates the guaranteed strength.
Referenced Documents: ASTM D7205: Standard Test Method for Tensile Properties of Fiber Reinforced Polymer Matrix Composite Bars.
Test Apparatus: The test apparatus shall comply with the requirements of ASTM D7205.
Test Specimens: Testing shall be performed on 0.6-in-diameter specimens.
Procedure: Tensile strength will be performed in accordance with ASTM D7209.
Calculations: Calculations will be performed in accordance with ASTM D7205.
Performance Requirements: Acceptance standard is $\geqq$ 2.30 kN/mm^2 or $\geqq$ 340 ksi, with a reported test result range of 2.42 to 2.68 kN/mm^2.
Report: Reporting will follow the guidance given in ASTM D7205.

Tensile Modulus of Elasticity

Scope: Indicates the rigidity of the strand.
Referenced Documents: ASTM D7205: Standard Test Method for Tensile Properties of Fiber Reinforced Polymer Matrix Composite Bars.
Test Apparatus: The test apparatus shall comply with the requirements of ASTM D7205.
Test Specimens: Testing shall be performed on 0.6-in-diameter specimens.
Procedure: Tensile modulus of elasticity testing will be performed in accordance with ASTM D7209.
Calculations: Calculations will be performed in accordance with ASTM D7205.
Performance Requirements: Acceptance standard is155 kN/mm^2 or 22481ksi, with a reported test result range of 135 to 160 kN /mm^2.
Report: Reporting will follow the guidance given in ASTM D7205.

Elongation
Scope: Indicates the degree of plastic deformation of the strand upon fracture.
Referenced Documents: ASTM D7205: Standard Test Method for Tensile Properties of Fiber Reinforced Polymer Matrix Composite Bars.
Test Apparatus: The test apparatus shall comply with the requirements of ASTM D7205.
Test Specimens: Testing shall be performed on 0.6-in-diameter specimens.
Procedure: Elongation will be performed in accordance with ASTM D7209 using a 2-in gauge length during testing.
Calculations: Calculations will be performed in accordance with ASTM D7205.
Performance Requirements: Acceptance standard is ≧1.3 %, with a reported test result range of 1.5% to 2.0%.
Report: Reporting will follow the guidance given in ASTM D7205.

Bond Test
Scope: Indicates the bond between the concrete and the strand.
Referenced Documents: ACI 440.3R.
Test Apparatus: The test apparatus shall comply with the requirements of ACI 440.3R.
Test Specimens: Testing shall be performed on 0.6-in-diameter specimens.
Procedure: Bond testing will be performed in accordance with ACI 440.3R.
Calculations: Calculations will be performed in accordance with ACI 440.3R.
Performance Requirements: Acceptance standard is equivalent to steel strand or better.
Report: Reporting will follow the guidance given in ACI 440.3R.

Glass Transition Test
Scope: Indicates the suitability and consistency of the resin.
Referenced Documents: ASTM E1356: Standard Test Method for Assignment of the Glass Transition Temperatures by Differential Scanning Calorimetry.
Test Apparatus: The test apparatus shall comply with the requirements of ASTM E1356.
Test Specimens: Testing shall be performed on 0.6-in-diameter specimens.
Procedure: Glass transition temperature testing will be performed in accordance with ASTM E1356.
Calculations: Calculations will be performed in accordance with ASTM E1356.
Performance Requirements: Acceptance standard is ≥ 212°F.
Report: Reporting will follow the guidance given in ASTM E1356.

Mass per Unit Length
Scope: This test is covered by Virginia Test Method (VTM) 139. This method covers the procedure to be used in determining mass per unit length (weight per foot) of carbon fiber reinforced polymer (CFRP) corrosion-free reinforcement. Indicates change or uniformity of the strand.
Referenced Documents: VTM 139: Determining the Mass per Unit Length (Weight per Foot) of Carbon Fiber Reinforced Polymer (CFRP) Corrosion-Free Reinforcement.
Test Apparatus: The test apparatus shall comply with the requirements of VTM 139.
Test Specimens: Testing shall be performed on 0.6-in-diameter specimens.
Procedure: Weight per foot testing will be performed in accordance with VTM 139.
Calculations: Calculations will be performed in accordance with VTM 139.

Performance Requirements: The acceptance standard is 221 g/m or 0.148 lb/ft, with the reported test result range of 217 to 226 g/m.
Report: Reporting will follow the guidance given in VTM 139.

Fiber Content
Scope: Indicates the quantity of fiber to matrix.
Referenced Documents: ASTM D2584: Standard Test Method for Ignition Loss of Cured Reinforced Resins or ASTM D3171: Standard Test Method for Constituent Content of Composite Materials, as determined by VDOT's Materials Division.
Test Apparatus: The test apparatus shall comply with the requirements of ASTM D2584 or ASTM D3171, as determined by VDOT's Materials Division.
Test Specimens: Testing shall be performed on a sample from a 0.6-in-diameter specimen.
Procedure: The test will be performed in accordance with ASTM D2584 or ASTM D3171, as determined by VDOT's Materials Division.
Calculations: Calculations will be performed in accordance with ASTM D2584 or ASTM D3171, as determined by VDOT's Materials Division.
Performance Requirements: The acceptance standard is >55% - volume or >70% - weight.
Report: Reporting will follow the guidance given in ASTM D2584 or ASTM D3171, as determined by VDOT's Materials Division.

Creep Rupture Strength
Scope: Provides an indication of the susceptibility of FRP bars to creep rupture, which is a phenomenon that can occur even when an FRP bar is maintained at a load that is below the static tensile strength of the bar.
Referenced Documents: ASTM D7337: Standard Test Method for Tensile Creep Rupture of Fiber Reinforced Polymer Matrix Composite Bars.
Test Apparatus: The test apparatus shall comply with the requirements of ASTM D7337.
Test Specimens: Testing shall be performed on a sample from a 0.6-in-diameter specimen.
Procedure: The test will be performed in accordance with ASTM D7337.
Calculations: Calculations will be performed in accordance with ASTM D7337.
Performance Requirements: The acceptance standard is ≥75% ultimate tensile strength.
Report: Reporting will follow the guidance given in ASTM D7337.

Pull-Out Test
Scope: Indicates the bond between the concrete and the strand.
Referenced Documents: ASTM A7913, ACI 440.3R, and VDOT SPEL 2017.
Test Apparatus: The test apparatus shall comply with the requirements of ASTM A7913.
Test Specimens: Testing shall be performed on 0.6-in-diameter specimen.
Procedure: Bond testing will be performed in accordance with ASTM A7913, with concrete strength at time of test ± 500 psi of f'c.
Calculations: Calculations will be performed in accordance with ASTM A7913.
Performance Requirements: The acceptance standard is 1,500 psi, with the reported test result range of 1,200 to 2,600 psi.
Report: Reporting will follow the guidance given in ASTM A7913.

Beam-End Test
Scope: Indicates the effect of curvatures on the strength loss of the strand.
Referenced Documents: ACI 440.3R.
Test Apparatus: The test apparatus shall comply with the requirements of ACI 440.3R.
Test Specimens: Testing shall be performed on 0.6-in-diameter specimens.
Procedure: Bond testing will be performed in accordance with ACI 440.3R with concrete strength at time of test ± 500 psi of f'c.
Calculations: Calculations will be performed in accordance with ACI 440.3R.
Acceptance Standard: Equivalent to steel strand or better.
Report: Reporting will follow the guidance given in ACI 440.3R.

Creep Test
Scope: Indicates the load for a time dependent deformation.
Referenced Documents: ASTM D7337: Standard Test Method for Tensile Creep Rupture of Fiber Reinforced Polymer Matrix Composite Bars.
Test Apparatus: The test apparatus shall comply with the requirements of ASTM D7337.
Test Specimens: Testing shall be performed on 0.6-in-diameter specimens.
Procedure: Creep testing will be performed in accordance with ASTM D7337.
Calculations: Calculations will be performed in accordance with ASTM D7337.
Acceptance Standard: Creep failure load ratio at 1 million hours = 0.85.
Report: Reporting will follow the guidance given in ASTM D7337.

Resistance to Alkaline Environment
Scope: Indicates the durability of the strand exposed to alkaline environment.
Referenced Documents: ASTM D7705: Standard Test Method for Alkali Resistance of Fiber Reinforced Polymer (FRP) Matrix Composite Bars used in Concrete Construction.
Test Apparatus: The test apparatus shall comply with the requirements of ASTM D7705.
Test Specimens: Testing shall be performed on 0.6-in-diameter specimens.
Procedure: Creep testing will be performed in accordance with ASTM D7705.

- King wire will be submerged in an alkaline solution of pH 13.
- King wire will be kept at 150°F the first 24 hours and then at room temperature thereafter.
- At 2 weeks, the king wire will be tested.

Calculations: Calculations will be performed in accordance with ASTM D7705.
Performance Requirements: The acceptance standard is ≥70% of ultimate tensile stress, based on ASTM D7705; Induce a tensile strain of 3000 microstrain using a set tensile stress; 3 months test duration tensile capacity retention.
Report: Reporting will follow the guidance given in ASTM D7705.

References

Virginia Department of Transportation. *Procedure for Qualification of Carbon Fiber Reinforced Polymer (CFRP) Bars for Placement on VDOT Special Products Evaluation List (SPEL).* Richmond, 2017. http://www.virginiadot.org/business/resources/Materials/CFRP_Qualification_Documents/CFRP_Pull-Out_and_Beam-End_Test_Descriptions.pdf. Accessed September 26, 2018.

Virginia Department of Transportation. *VTM 139: Determining the Mass per Unit Length (Weight per Foot) of Carbon Fiber Reinforced Polymer (CFRP) Corrosion-Free Reinforcement.* Richmond, 2018. http://www.virginiadot.org/business/resources/Materials/bu-mat-VTMs.pdf. Accessed September 26, 2018.